Effects of successive peak-flow events on hyporheic exchange and residence times

Tanu Singh[1,7], Jesus D. Gomez-Velez[2], Liwen Wu[3,4], Anders Wörman[5], David M. Hannah[1], Stefan Krause[1,6]

[1]School of Geography, Earth and Environmental Sciences, University of Birmingham,UK.
[2]Department of Civil and Environmental Engineering, Vanderbilt University, Nashville, TN, USA.
[3]Department of Ecohydrology, Leibniz-Institute of Freshwater Ecology and Inland Fisheries, Berlin, Germany.
[4]Geography Department, Humboldt-University, Berlin, Germany
[5]Division of River Engineering, Royal Institute of Technology, Stockholm, Sweden
[6]University Claude Bernard Lyon 1, LEHNA - Laboratory of Ecology of Natural and Man-Impacted Hydrosystems, Lyon, France
[7]Now at Department of Numerical Mathematics, Technical University of Munich, Garching, Germany.

Key Points:

- Dynamic response of hyporheic exchange fluxes, residence times and breakthrough curves to successive peak-flow events is investigated
- Increased time-lag between successive flow peaks cause higher temporal variability in mean residence times of hyporheic water
- Two events can be treated separately if the occurrence of subsequent event is longer than the memory of the system from the antecedent event

Corresponding author: Tanu Singh, tanu.singh@tum.de

This article has been accepted for publication and undergone full peer review but has not been through the copyediting, typesetting, pagination and proofreading process which may lead to differences between this version and the Version of Record. Please cite this article as doi: 10.1029/2020WR027113

Abstract

Hyporheic exchange is a crucial control of the type and rates of streambed biogeochemical processes, including metabolism, respiration, nutrient turnover, and the transformation of pollutants. Previous work has shown that increasing discharge during an individual peak-flow event strengthens biogeochemical turnover by enhancing the exchange of water and dissolved solutes. However, due to the non-steady nature of the exchange process, successive peak-flow events do not exhibit proportional variations in residence time and turnover, and in some cases, can reduce the hyporheic zones' biogeochemical potential. Here, we used a process-based model to explore the role of successive peak-flow events on the flow and transport characteristics of bedform-induced hyporheic exchange. We conducted a systematic analysis of the impacts of the events' magnitude, duration, and time between peaks in the hyporheic zone's fluxes, penetration, and residence times. The relative contribution of each event to the transport of solutes across the sediment-water interface was inferred from transport simulations of a conservative solute. In addition to temporal variations in the hyporheic flow field, our results demonstrate that the separation between two events determines the temporal evolution of residence time, and that event time lags longer than the memory of the system result in successive events that can be treated independently. This study highlights the importance of discharge variability in the dynamics of hyporheic exchange and its potential implications for biogeochemical transformations and fate of contaminants along river corridors.

1 Introduction

River discharge and stage are characterized by significant temporal variability and frequent peak-flow events (Bernard-Jannin et al., 2016; Gomez-Velez, Wilson, Cardenas, & Harvey, 2017; Krause et al., 2011; Mojarrad, Betterle, Singh, Olid, & Wörman, 2019; Salazar, Vargas, Nájera, Seguel, & Casanova, 2014; Sawyer, Cardenas, Bomar, & Mackey, 2009; Singh et al., 2019; Trauth & Fleckenstein, 2017; Vivoni, Bowman, Wyckoff, Jakubowski, & Richards, 2006; Wu et al., 2018). This variability results from natural drivers (snow and precipitation events) and anthropogenic interference (such as artificial inputs from waste water treatment plants or dam operations). Perturbations in river stage and discharge —alter the pressure distributions at the interface between the water column and the streambed, the main driver for hyporheic exchange and thus lead to exchange fluxes several orders of magnitude higher than the ones under the base flow conditions (Gomez-Velez et al., 2017; Singh et al., 2019; Wu et al., 2018). In addition to river stage fluctuations and pressure variations, continuous exchange of water, solutes and energy between the water column and the hyporheic zone is controlled by interactions between geomorphological settings, channel gradient, hydraulic conductivity, sediment heterogeneity and spatial variability in heads at the sediment-water interface (SWI) and preferential flow paths (Gomez-Velez & Harvey, 2014; Gomez-Velez, Krause, & Wilson, 2014; Lotts & Hester, 2020; Marzadri, Tonina, Bellin, & Valli, 2016; Menichino & Hester, 2015; Tonina & Buffington, 2011). Interactions between these driving mechanisms determine the hydrodynamics and residence times within the hyporheic zone.

Successive peak-flow events can cause variability in physio-chemical characteristics of streambed fluids (Bruno, Maiolini, Carolli, & Silveri, 2009; Fritz & Arntzen, 2007; Hinton, Schiff, & English, 1997; Inamdar, Christopher, & Mitchell, 2004; Krause et al., 2011). The main impacts of peak-flow events relate to the activation of deeper subsurface flow paths, enhanced reactivity owing to the faster transport of solutes into the reactive zones and contaminant attenuation. For example, when denitrification in anaerobic zones of the hyporheic zone is limited by the supply of labile dissolved organic carbon (DOC) (Zarnetske, Haggerty, Wondzell, & Baker, 2011), peak-flow events can facilitate higher and faster transport of DOC into the streambed and thus, enhance nitrogen cycling (Hinton et al., 1997; Inamdar et al., 2004). Fritz and Arntzen (2007) found that the higher influx of river water during increased water levels resulted in lower uranium concentrations due to dilution effects. Bruno et al. (2009) showed that peak-flow event induced disturbance can have negative effects for hyporheic invertebrates because sharp increase in discharge can lead to scouring, disturbing the benthic invertebrates and salmonid eggs, and eventually impacting overall ecosystem functioning.

Previous modelling studies have analyzed the impact of dynamic stream flow on groundwater - surface water exchange flow processes and hyporheic exchange (Boano, Revelli, & Ridolfi, 2013; Dudley-Southern & Binley, 2015; Malzone, Anseeuw, Lowry, & Allen-King, 2016; Malzone, Lowry, & Ward, 2016; McCallum & Shanafield, 2016; Schmadel, Ward, Lowry, & Malzone, 2016; Ward et al., 2013; Ward, Schmadel, & Wondzell, 2018), and for this, primarily focused on the effect of individual discharge events on hyporheic exchange processes (Gomez-Velez et al., 2017; Liang, Zhan, & Schilling, 2018; Singh et al., 2019; Trauth & Fleckenstein, 2017; Wu et al., 2018). These studies led to the identification of dominant drivers and controls of hyporheic exchange flows during transient stream flow conditions. For example, Harvey et al. (2012) found that larger magnitude and longer-lasting events have higher potential to activate hyporheic flow paths and engage in solute and fine particulate transport. The modelling of dynamic hyporheic exchange fluxes by Malzone, Lowry, and Ward (2016) showed that the volume of the hyporheic zone and the hyporheic exchange fluxes are modulated by annual and storm-induced groundwater fluctuations. Schmadel et al. (2016) investigated the importance of diel hydrologic fluctuation and controls such as hillslope lag, amplitude of the hillslope and cross-valley and down-valley slopes on hyporheic flow path and residence times. McCallum and Shanafield (2016) found alterations in the residence time distributions of bank inflows and outflows for different flow events, and Gomez-Velez et al. (2017) explored the role of high discharge events on the spatial and temporal evolution of river bank storage and sinuosity-driven hyporheic exchange. In addition, a field-based study incorporating successive storm events by Dudley-Southern and Binley (2015) showed that such events could lead to a reversal of the vertical hydraulic gradient and can enhance mixing up to 30 cm within the streambed. Similar outcomes were also found by Krause and Bronstert (2007) and Munz, Krause, Tecklenburg, and Binley (2011). To the authors' knowledge, none of the previous modelling studies incorporated the effects of successive hydrological events as they commonly occur in natural settings (e.g. driven by storm events, cyclic behavior of waste-water treatment plants,and dam operations), therefore mechanistic understanding of the impacts of successive peak-flow events remains elusive. Moreover, the effect of the interaction between two successive events on water and solute transport within the hyporheic zone remains largely unaccounted in these studies.

The goals of this multi-parametric study are to compare and contrast the hydrodynamics and solute transport characteristics of hyporheic exchange driven by a single peak-flow event and two consecutive flood events. This is done by systematically modeling the flow of water, transport of a conservative tracer, and the evolution of mean residence times. We provide a systematic approach to decipher the potential impacts of successive peak-flow events on hyporheic exchange flows, using reduced-complexity models of idealized, uniform and single types of bedform-induced hyporheic exchange. The term *reduced-complexity* indicates that the model formulation assumes and captures first-order drivers and controls of the exchange process, ignoring some of higher-order complexities such as heterogeneity in the sediments (Gomez-Velez et al., 2014). These analyses allow us to develop a comprehensive understanding from a large number of simulations enabled by the reduced computational effort. We evaluate the impacts of two successive peak-flow events, the first event is referred to as *antecedent peak-flow event*, and second one as the *subsequent peak-flow event*, by studying the effects of three different parameters, namely (i) the time lag between two peak-flow events (t_{lag}); (ii) the magnitude (H_{p_1}-H_{p_2}); and (iii) the duration of subsequent flow event (t_{d_1}-t_{d_2}) in relation to the preceding event. This study provides important mechanistic understanding of the flow and transport behaviour in dynamically forced hyporhiec zones,with relevance for biogeochemical cycling at the interface of surface and groundwater systems. Our results can theefore be used as a guide for designing field experiments and the interpretation of tracer studies in dynamic flow systems, as well as interpretation of hyporheic zone turnover efficiencies.

2 Methodology

A process-based model was developed in this study and used for performing model simulations following an approach of six major steps (1) set-up of simulation framework including streambed sediment geometry and parameterization of properties; (2) generation of successive peak-flow event stage hydrograph; (3) inclusion of flow in porous media model; (4) solute transport model to track

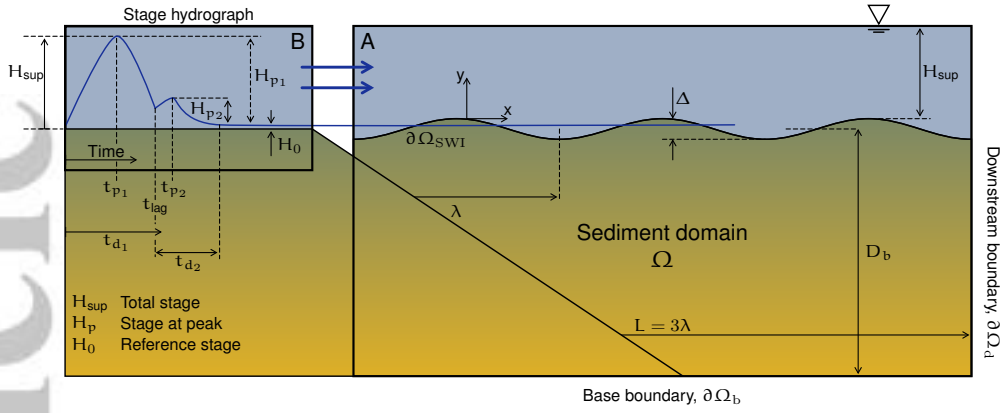

Figure 1. Schematic representation of the reduced-complexity model. A. depicts the sediment domain (Ω) which is assumed homogeneous and isotropic. Hyporheic exchange is driven by streambed topography, channel gradient and time-varying stage. B describes the prescribed head distribution which is imposed along the SWI ($\partial\Omega_{SWI}$). Periodic boundary conditions are assumed for the lateral boundaries ($\partial\Omega_u$ and $\partial\Omega_d$), horizontal ambient flow is assumed proportional to the channel slope, and the base of the model domain ($\partial\Omega_b$) is assumed impervious. Flow direction is from left to right.

the response of hyporheic exchange and dynamic hyporheic zone development; (5) implementation and simulation of residence time model; and (6) simulation of numerical breakthrough curves and development of model scenarios.

2.1 Conceptual model

We use a simplified conceptualization of a streambed-river interface to systematically explore the impact of successive peak-flow events on bedform-driven hyporheic exchange (Elliott & Brooks, 1997; Singh et al., 2019; Stonedahl, Harvey, Wörman, Salehin, & Packman, 2010). For this purpose, we implement detailed flow, transport and residence time models in the model domain. The modeling domain (Ω) represents homogeneous and isotropic stream sediments. It is bounded at the top by the SWI ($\partial\Omega_{SWI}$), which is assumed sinusoidal $Z_{\mathrm{SWI}}(x) = \frac{\Delta}{2}\sin(\frac{2\pi x}{\lambda})$ where Δ [L] (= 0.1 m) and λ [L] (= 1 m) are the characteristic amplitude and wavelength of the bedform, respectively (see Figure 1). The total length and depth of the modelling domain are $L = 3\,\lambda$ and $D_b = 5\,\lambda$, respectively. At the bottom, the model domain is bounded by a horizontal boundary ($\partial\Omega_b$) and at sides by the vertical boundaries ($\partial\Omega_u$ and $\partial\Omega_d$). These dimensions are selected to avoid boundary effects in the numerical simulations.

The numerical solution of the proposed model is implemented into COMSOL Multiphysics for simulation. Mesh independent solutions are achieved with a resultant mesh of approximately forty-thousand triangular elements with telescopic refinement closer to the sediment-water interface. This refinement is required in order to capture the effect of local, fast-flowing hyporheic circulation cells and have accurate flux integrals along the boundaries.

2.2 Successive peak-flow events hydrograph generation

Individual peak-flow pulses or successions thereof are used as simplification to represent the dynamic nature of river discharge. The deterministic stage hydrograph is modeled with an asymmetric

curve as proposed by Cooper and Rorabaugh (1963):

$$H_{\text{generic}}(t) = \begin{cases} H_0 + H_p\, e^{-\delta(t-t_{lag})}\, \dfrac{[1-\cos(wt)]}{[1-\cos(wt_p)]} & \text{if} \quad t > t_{lag}, \quad \& \quad t < t_d + t_{lag} \\ H_0 & \text{otherwise} \end{cases} \tag{1}$$

where H_0 is the stage at baseflow conditions [L], H_p is the maximum rise of stream stage [L], t_p is the time-to-peak of the event [T], t_{lag} is the time of the occurrence of the subsequent event defined by the Equation (10) [T], t_d is the duration of the peak-flow event [T], $w = 2\pi/t_d$ is the frequency of the event [T^{-1}], and $\delta = w\cot(wt_p/2)$ is a constant that determines the degree of asymmetry [T^{-1}].

We use the $H_{\text{generic}}(t)$ to create hydrographs with successive peak-flow events

$$H_{sup}(t) = H_{\text{generic}}(t, H_{p1}, t_{p1}, t_{d1}, 0) + H_{\text{generic}}(t, H_{p2}, t_{p2}, t_{d2}, t_{lag}) - H_0 \tag{2}$$

where H_{p1}, t_{p1} and t_{d1} describe the antecedent peak-flow event and H_{p2}, t_{p2}, t_{d2} and t_{lag} describe the subsequent peak-flow event. Note that for all the explored scenarios, antecedent peak-flow event commence at $t = 0$. For convenience, from here t_{lag} is used to define the lag between two peak-flow events and the time at which subsequent event commences, t_{d2} is used to describe the time at which duration of the subsequent event ends (*i.e.* at $t_{lag} + t_{d2}$) and t_{p2} for the time at which peak for the subsequent event occurs (*i.e.* at $t_{lag} + t_{p2}$).

With estimated the time-varying river stage ($H_{sup}(t)$), we describe the pressure distribution at the SWI ($\partial\Omega_{SWI}$). For simplicity, we use an expression for prescribed head distribution that assumes a linear combination of head fluctuations induced by large- and small-scale bed topography (Stonedahl et al., 2010; Wörman, Packman, Marklund, Harvey, & Stone, 2006):

$$h_{SWI}(x,t) = -S\,x + H_{sup}(t) + \frac{2\,h_d(t)}{\Delta}\, Z_{SWI}\left(x + \frac{\lambda}{4}\right) \tag{3}$$

where S is channel slope, $H_{sup}(t)$ [L] is the time-varying river stage, $Z_{SWI}(x)$ is the function describing the bed topography, and $h_d(t)$ is the intensity of the dynamic head fluctuations (Elliott & Brooks, 1997),

$$h_d(t) = 0.28\frac{U_s(t)^2}{2g} \begin{cases} \left(\dfrac{\Delta}{0.34\,H_{sup}(t)}\right)^{3/8} & \text{for} \quad \dfrac{\Delta}{H_{sup}(t)} \leqslant 0.34, \\ \left(\dfrac{\Delta}{0.34\,H_{sup}(t)}\right)^{3/2} & \text{for} \quad \dfrac{\Delta}{H_{sup}(t)} > 0.34, \end{cases} \tag{4}$$

where the mean velocity is estimated with the Chezy equation for a rectangular channel as $U_s(t) = M^{-1}H_s(t)^{2/3}S^{1/2}$ with M is the Manning coefficient [$L^{-1/3}T$] (Dingman, 2009). Notice that the pressure distribution at the sediment-water interface is a function of both space x and time t, where the temporal fluctuations are induced by the peak-flow events (see Equation 3).

2.3 Flow model

Flow within the domain is driven by pressure gradients at the sediment-water interface ($\partial\Omega_{SWI}$). Neglecting the storage term, a reasonable assumption for submerged channel sediments, flow within the domain is described by the following version of the groundwater flow equation and Darcy's law

$$\nabla \cdot \left[\rho\frac{\kappa}{\mu}\left(\nabla p + \rho g \nabla z\right)\right] = 0 \tag{5}$$

where $\mathbf{x} = (x, y)$ is the spatial location vector [L], $p(\mathbf{x}, t)$ is pressure [$ML^{-1}T^{-2}$], g is the acceleration due to gravity [LT^{-2}], κ is the permeability [L^2], ρ is fluid density [ML^{-3}], μ_d is fluid dynamic

viscosity [$ML^{-1}T^{-1}$], $h = \frac{p}{\rho g} + z$ is hydraulic head [L], and Darcy velocity is $\mathbf{q} = -\frac{\kappa}{\mu}(\nabla p + \rho g \nabla z))$ [LT^{-1}].

Assuming that bedforms repeat periodically along the channel, we implemented a periodic boundary condition for the lateral boundaries ($\partial\Omega_u$ and $\partial\Omega_d$; $p(x = -L, y, t) = p(x = 2L, y, t) + \rho g[h_{SWI}(x = -L, t) - h_{SWI}(x = 2L, t)]$). Under neutral groundwater conditions (*i.e.* without gaining and losing groundwater conditions), the only groundwater flow constraining the hyporheic zone is the ambient groundwater flow driven by the channel gradient (*i.e.* horizontal under-flow component), and therefore no-flow is assumed at the lower model boundary ($\partial\Omega_b$). The depth of this boundary (d_b) was selected to minimize boundary effects. Finally, the solution under steady state (*i.e.* , baseflow conditions) is used as the initial condition for the transient simulations (*i.e.* , during the peak-flow event). This method of calculating pressure distribution at the SWI reproduces reasonable observations. It also allows the exploration of large number of scenarios with fewer complexities when implemented in the model, and with reduced computational demand.

The sediment-water interface ($\partial\Omega_{SWI}$) can be discretized into inflow ($\partial\Omega_{IN} = \{\mathbf{x} \mid (\mathbf{n} \cdot \mathbf{q} < 0) \ \wedge (\mathbf{x} \in \partial\Omega_{SWI})\}$) and outflow sub-boundaries ($\partial\Omega_{OUT} = \{\mathbf{x} \mid (\mathbf{n} \cdot \mathbf{q} > 0) \ \wedge (\mathbf{x} \in \partial\Omega_{SWI})\}$) such that $\partial\Omega_{SWI} = \partial\Omega_{IN} \cup \partial\Omega_{OUT}$ with $\mathbf{n}$ an outward vector normal to the boundary. Notice that these boundaries are dynamic in nature, contracting and expanding with variations in the time-varying river stage, $H_{sup}(t)$.

2.4 Solute transport model and delineation of the hyporheic zone

The advection-dispersion equation (ADE) is used to model the transport of conservative solutes within the streambed sediments

$$\theta \frac{\partial C}{\partial t} = \nabla \cdot (\mathbf{D}\nabla C) - \nabla \cdot (\mathbf{q}C) \tag{6}$$

where C is concentration [ML^{-3}], $\mathbf{q}$ is the Darcy flux [LT^{-1}], and $\mathbf{D} = \{D_{ij}\}$ is the dispersion-diffusion tensor defined as Bear (1972):

$$D_{ij} = \alpha_T |\mathbf{q}| \delta_{ij} + (\alpha_L - \alpha_T) \frac{q_i \, q_j}{|\mathbf{q}|} + \frac{\theta}{\xi_m} D_m \tag{7}$$

with α_T (0.05 m) and α_L (α_T/10) the transverse and longitudinal dispersivities [L] (Gomez-Velez & Harvey, 2014; Gomez-Velez et al., 2017), D_m the effective molecular self-diffusion coefficient, $\xi_m = \theta^{-1/3}$ is the fluid tortuosity (defined here with the Millington and Quirk model (Millington & Quirk, 1961)), and δ_{ij} is the Kronecker delta function.

Modelling the transport of a conservative tracer allows us to explore the mixing and extent of the hyporheic zone. We assume that the concentration of the tracer in the stream water column is C_s, and therefore a prescribed boundary condition $C(\mathbf{x}, t) = C_s$ is used along the SWI's inflow areas ($\partial\Omega_{IN}$). Outflow areas ($\partial\Omega_{OUT}$) along the SWI are advective boundaries where $\mathbf{n} \cdot (\mathbf{D}\nabla C) = 0$. Lateral boundaries ($\partial\Omega_u$ and $\partial\Omega_d$) are periodic boundaries $C(x = -L, y) = C(x = 2L, y)$ and the bottom boundary ($\partial\Omega_b$) is a no-flow boundary $\mathbf{n} \cdot (\mathbf{q}C - \mathbf{D}\nabla C) = 0$. An initial condition for the concentration field is obtained from a steady-state simulation of the transport model (Eq. (6)) under baseflow conditions (*i.e.* , $H_s = H_0$). In this case, the hyporheic zone is defined as the zone with at least 90% of the pore water originated from the stream (*i.e.* , $C \geq 0.9C_s$). This definition is similar to the one proposed by Triska, Kennedy, Avanzino, Zellweger, and Bencala (1989) and Gomez-Velez et al. (2014, 2017). Throughout the manuscript, we refer to this definition as the *biogeochemical definition of the hyporheic zone*.

2.5 Residence time model

The hyporheic zone residence time describes the time that water and solutes are exposed to the stream sediment biogeochemical conditions. Here, we evaluate the impacts of transient flow,

driven by successive peak-flow event, on the first moment of the hyporheic zone's residence time distribution. To this end, we use the approach outlined in Gomez-Velez, Wilson, and Cardenas (2012), Gomez-Velez and Wilson (2013), and Gomez-Velez et al. (2017) where the moment of the residence time distribution are described by an ADE of the form

$$\frac{\partial(\theta a_1)}{\partial t} = \nabla \cdot (\theta \mathbf{D} \nabla a_1) - \nabla \cdot (\mathbf{q} \theta a_1) + \theta a_0 \tag{8a}$$

$$a_1(\mathbf{x}, t) = 0 \quad \text{on } \partial\Omega_{IN} \tag{8b}$$

$$\mathbf{n} \cdot (\theta \mathbf{D} \nabla a_1) = 0 \quad \text{on } \partial\Omega_{OUT} \tag{8c}$$

$$a_1(x = -L, y) = a_1(x = 2L, y) \text{ for } \partial\Omega_u \text{ and } \partial\Omega_d \tag{8d}$$

$$\mathbf{n} \cdot (\mathbf{q} a_1 - \mathbf{D} \nabla a_1) = 0 \quad \text{on } \partial\Omega_b \tag{8e}$$

$$a_1(\mathbf{x}, t = t_0) = a_{10} = \int_0^\infty \tau \Psi_0(\mathbf{x}, \tau) \, \mathrm{d}\tau \tag{8f}$$

where $\mathbf{q}$ is the Darcy flux [LT^{-1}], $a_0 = 1$, θ is the effective porosity [-], $\mathbf{D} = \{D_{ij}\}$ is the dispersion-diffusion tensor (Bear, 1972) and $a_1(\mathbf{x}, t)$ [T] is the first moment of the residence time distribution $\Psi(\mathbf{x}, t, \tau)$ [T^{-1}], which is defined as

$$a_1(\mathbf{x}, t) = \int_0^\infty \tau \Psi(\mathbf{x}, t, \tau) \, \mathrm{d}\tau, \text{ for } n = 1, 2, \ldots \tag{9}$$

Initial and boundary conditions are defined following the approach of Gomez-Velez and Wilson (2013) and Gomez-Velez et al. (2017). Similar to the conservative transport model, the initial distribution of the first moment of the residence time distribution (mean residence time) were estimated under steady baseflow conditions.

2.6 Numerical breakthrough curves and scenarios

To model the breakthrough curves, firstly the advection-dispersion equation is implemented on multiple conservative tracers. Multiple conservative tracers are deployed to potentially estimate relative contributions by not only antecedent and subsequent events individually but also when the events are superimposed. We define the time of the occurrence of the subsequent event (t_{lag}) by the equation

$$t_{lag} = t_{p1} + \eta(t_{d1} - t_{p1}) \tag{10}$$

where η = 1/4, 2/4, 3/4, 4/4, 5/4 and 6/4. Depending on the values of η describing the time lag between both events, tracking of the mixing between the two events would need deployment of two or three conservative tracers. Following are the formulated cases (See Figure 2):

Case I: $\eta < 1, t_{lag} < t_{d1}, t_{d1} \geq t_{lag} + t_{d2}$
Case II: $\eta < 1, t_{lag} < t_{d1}, t_{d1} < t_{lag} + t_{d2}$
Case III: $\eta \geq 1, t_{lag} \geq t_{d1}$

To track the mixing for Case I, two tracers are injected namely c_1 and c_2. The tracers are described by the piece-wise function where $c_1 = c_s$ (where we assume c_s is the concentration of the conservative tracer in the water column) when the antecedent event is active or the rise in stage is caused by the antecedent, $c_2 = c_s$ when both the events are active i.e. the stage rise is due to combined effect of the two events and finally we use $c_3 = c_s$ for stage rise due to the subsequent event only (see Figure 2 for further clarification).

For the tracer entering the sediment-water interface *i.e.* $\partial\Omega_{IN}$, the total mass that entered the system is estimated as

$$M_{in} = \int_a^b \left[\int_{\partial\Omega_{IN}} (\mathbf{n}.\mathbf{q}) c \, \mathrm{d}x \right] \mathrm{d}t \tag{11}$$

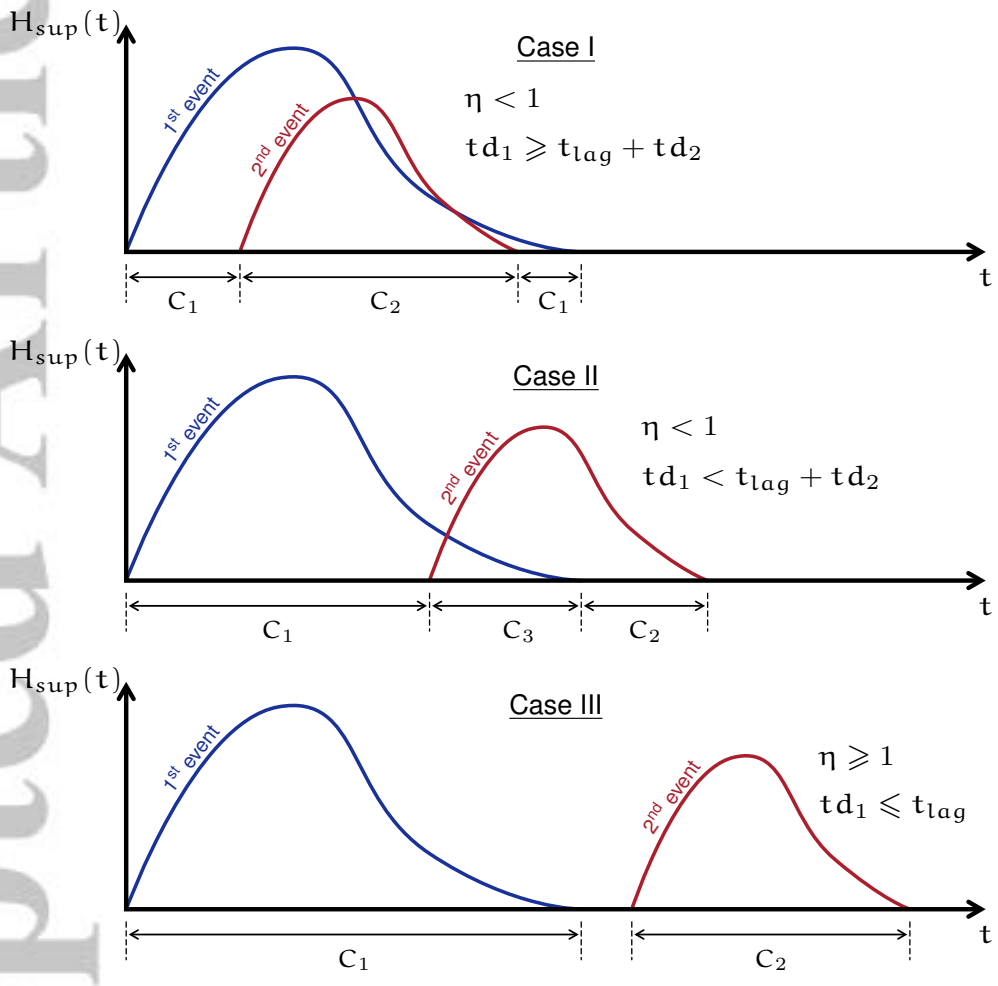

Figure 2. Depiction of the deployment of conservative tracers depending on the lag between two events t_{lag} (See Equation 10). c_1, c_2 and c_3 are the conservative tracers made active depending on the occurrence of the subsequent event. Cases I and II constitute the scenarios with superimposition or overlapping of two events whereas Case III represents scenarios with no overlapping of the two peak-flow events.

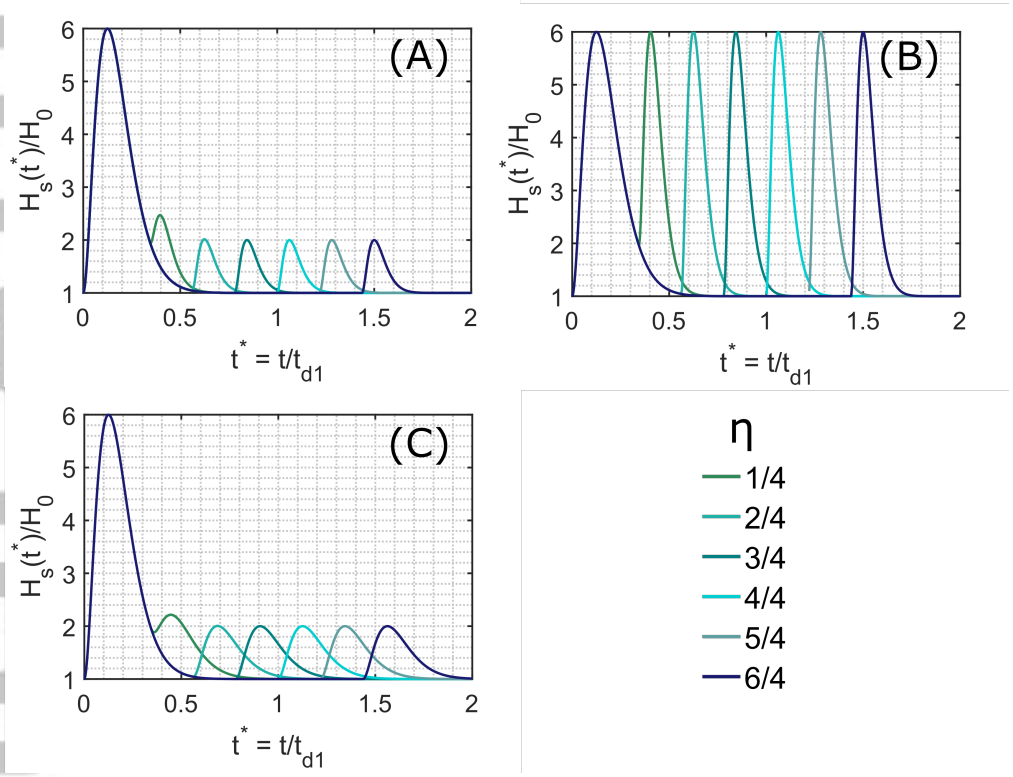

Figure 3. Depiction of dimensionless stage hydrographs. The antecedent peak-flow event is of higher magnitude and is identical for all the scenarios. For (A) *i.e.* Category 1, the subsequent peak-flow event is of shorter magnitude and occurs at t_{lag} defined by Equation 1 ($H_{p_1} > H_{p_2}$ and $t_{d_1} > t_{d_2}$). As shown, scenarios with η = 1/4, 2/4 and 3/4 the two events are superimposed. For the scenarios with η = 4/4, 5/4 and 6/4, the subsequent event occurs after the duration of the antecedent event. For (B) *i.e.* Category 2, $H_{p_1} = H_{p_2}$ and $t_{d_1} > t_{d_2}$ and for (C) *i.e.* Category 3, $H_{p_1} > H_{p_2}$ and $t_{d_1} = t_{d_2}$

where $\partial\Omega_{IN}$ is the inflow boundary at the sediment-water interface. The mass leaving the hyporheic zone is given by

$$m_{out} = \int_{\partial\Omega_{OUT}} (\mathbf{n}.\mathbf{q})c \, \mathrm{d}x \tag{12}$$

Finally the cumulative mass (or recovery) gives the breakthrough curve (BTC) estimated by the following mathematical statement

$$BTC(t) = \frac{\int_0^t m_{out} \, \mathrm{d}t}{M_{in}} \tag{13}$$

All the scenarios used for the simulations have the same duration (t_{d_1}) and magnitude of the antecedent event (H_{p_1}; see Figure 3). Time to peak of the antecedent event $t_{p_1} = Sk_1 \times t_{d_1}$ and time to peak for the subsequent event $t_{p_2} = Sk_1 \times t_{d_2}$, where $Sk_1 = 1/8$. Category 1 represent the scenarios with magnitude of the subsequent event (H_{p_2}) less than the magnitude of the antecedent event (H_{p_1}) and duration of the subsequent event (t_{d_2}) is less than the duration of the antecedent event (t_{d_1}) (Figure 3 (A)). Category 2 (Figure 3 (B)) corresponds to scenarios where the magnitude of the two events is the same ($H_{p_1} = H_{p_2}$), and the duration of the subsequent event is less than or equal to the duration of the antecedent event ($t_{d_2} \leq t_{d_1}$). Finally, Category 3 (Figure 3C) corresponds to scenarios where the magnitude of the subsequent event is lower than the one of the antecedent event ($H_{p_2} < H_{p_1}$), and the duration of events is the same ($t_{d_2} = t_{d_1}$). (Figure 3 (C)).

3 Results and Discussion

3.1 Hyporheic Flow Field and Extent

The peak-flow event induced pressure distributions along the sediment-water interface vary dynamically. The temporal evolution of flow fields are illustrated in Figure 4. Time $t \leq 0$ represents the base flow conditions and time $t \leq t_{d_2}$ represents the dynamics during the superimposed event for the scenario $\eta = 3/4$. The hyporheic zone dynamically expands and contracts during these events, with maximum expansion at $t = t_{p_1}$ due to the large magnitude of the antecedent event. Also, the hyporheic zone expands at $t = t_{p_2}$; however the magnitude of the expansion is relatively less than compared to $t = t_{p_1}$ due to the smaller magnitude of the subsequent event in the illustrated example. The magnitude and duration of the events determine the dynamic changes in the flow field.

We also use the biogeochemical definition to define and illustrate the hyporheic zone (see the black line in Figure 4). This is numerically achieved by introduction of a conservative tracer and tracking its transportation in the streambed. The contour line delineating the biogeochemically defined hyporheic zone with at least 90% of the water originating from the stream indicates that both, hyporheic zone shape and size vary considerably for different times. However these patterns tend to be more stable than compared to the variations in the flow field. Such behaviour can be explained by the flow field instantaneously propagating with pressure fluctuations at the sediment-water interface. On the other hand, the hyporheic zone extent based on biogeochemical definition takes into consideration transport and retention processes within the hyporheic zone. Observations demonstrate the variability in the hyporheic zone extent showing considerable change for $t = t_{p_1}$, followed by $t = t_{p_2}$, both linked to maximum rise in stage.

Another characteristic behaviour demonstrated by the model results is the horizontal and longitudinal movement of stagnation zones (in each subplot of Figure 4) which would also be observed in the case of single peak-flow event (Singh et al., 2019). These are the regions or locations where the absolute Darcy velocity is zero or near-zero to form stagnant zones. The presence of stagnation zones is dependent on the existence of the counter-directional local flow systems (Jiang, Wang, Wan, & Ge, 2011). Dynamic stagnation zones are usually characterised as reactive hotspots, playing a primary role in types and rates biogeochemical transformations, such as the reduction of nitrates and nitrites in the nitrogen cycle (Krause, Boano, Cuthbert, Fleckenstein, & Lewandowski, 2014; Pinay

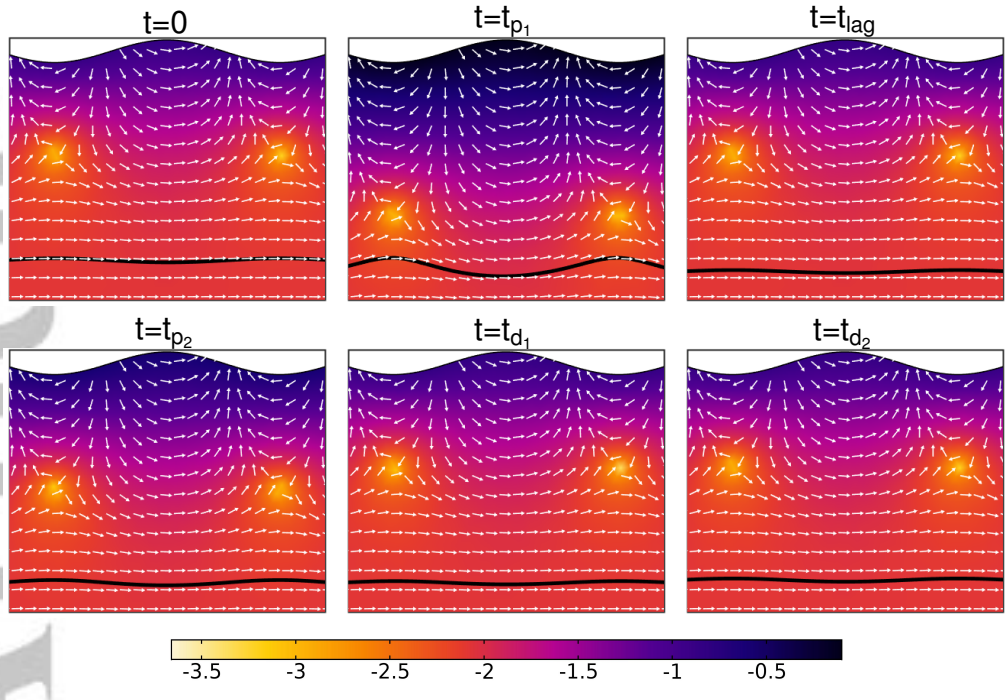

Figure 4. Snapshots of the flow field (white arrows represent direction and not proportional to magnitude) and hyporheic zone extent using the biogeochemical definition (black line) within the sediment domain. Surface represents the magnitude of Darcy flux vector (in log scale m/d) for time at $t = 0$, $t = t_{p_1}$, $t = t_{lag}$, $t = t_{p_2}$, $t = t_{d_1}$ and $t = t_{d_2}$ for the scenario with $\eta = 3/4$ within Category 1 simulations. ($\Delta/\lambda = 0.1$, $S = 0.001$)

et al., 2015). Furthermore, the dynamic variations in the flow field and the stagnation points bears relevance for fate and transport of contaminants in river-corridors.

3.2 Flux-weighted mean residence time

A representative value of residence times for the hyporheic exchange process is estimated by flux-weighting the modeled mean residence time along the sections of the SWI discharging hyporheic water into the stream (described in the residence time model). The mean residence time, μ corresponds to the first central moment, a_1. Here we estimate flux-weighted mean residence time, μ^*_τ relative to baseflow conditions.

Flux-weighted mean residence time (μ^*_τ) slightly increases at first with the antecedent peak-flow event (Figure 5, 6 and 7). This behaviour is caused by the first high flush in all scenarios expanding the hyporheic zones, penetrating deeper into the sediments and discharging older hyporheic waters, reaching its maximum before an event's time to peak. Increased mean residence time of water discharged from the hyporheic zones for a short period of time is followed by progressive discharge of younger hyporheic waters due to activation of short flow paths closer to the sediment-water interface. This is in line with findings of Singh et al. (2019) and Gomez-Velez et al. (2017).

The antecedent peak-flow event is followed by the low magnitude (Figures 5 and 7) and high magnitude subsequent peak-flow event (Figure 6) which is superimposed for the cases with $\eta = 1/4, 2/4$ and $3/4$ (first row of Figure 5 and 6) and separated for $\eta = 4/4, 5/4$ and $6/4$ (second row of Figure 5). This event disturbs the system causing variability, preventing the system to attain base-flow conditions for a certain period of time depending on the values on η, magnitude and duration of the subsequent peak-flow event. This leads to discharge of relatively older water (compared to reference

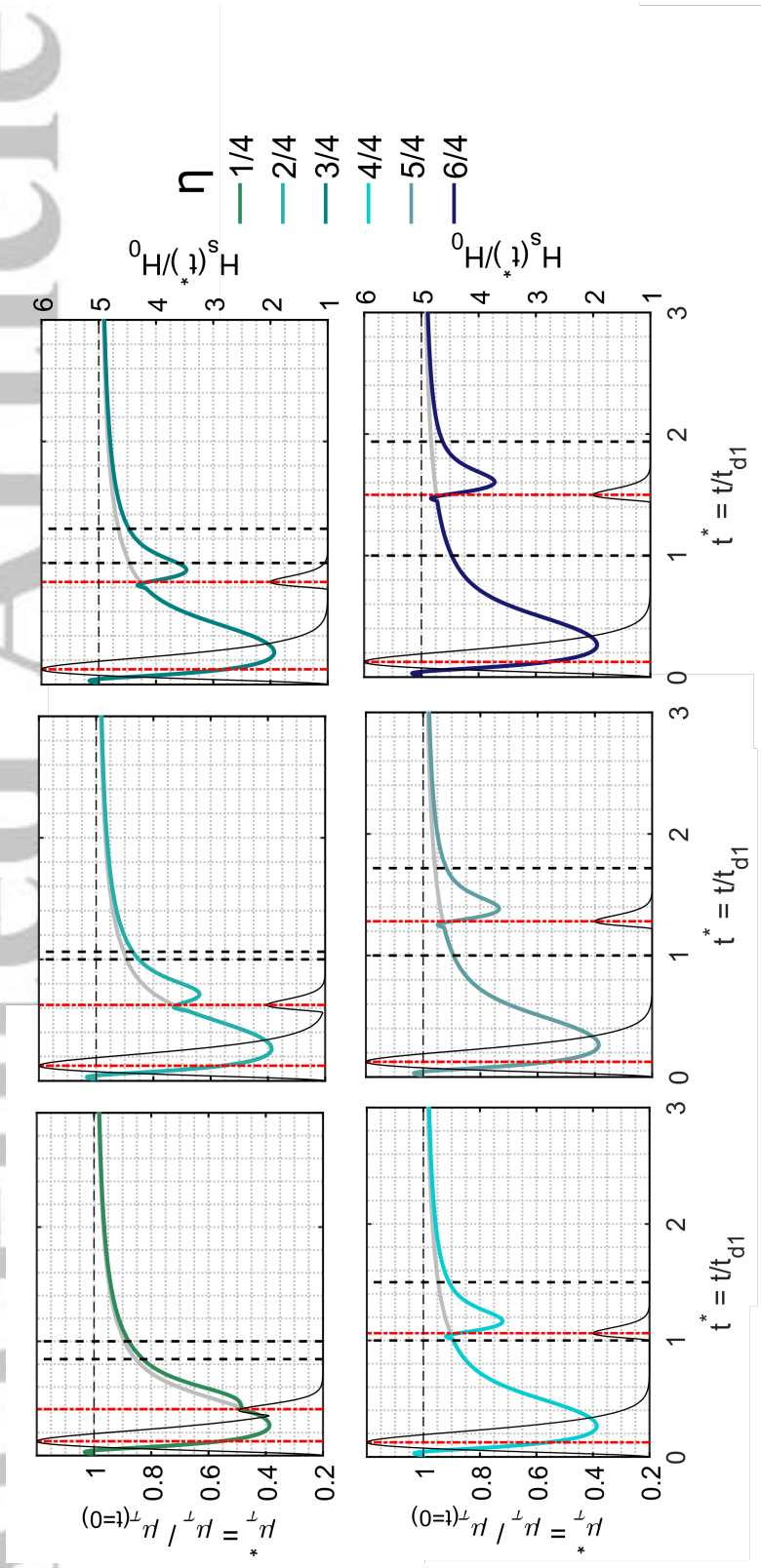

Figure 5. Temporal evolution of flux-weighted residence time μ_τ^* of hyporheic waters leaving the sediment-water interface, as a function of dimensionless time. Category 1 scenarios are shown where $H_{p_1} > H_{p_2}$ and $t_{d_1} > t_{d_2}$. Vertical red lines and black lines correspond to time-to-peak and duration of the events respectively. Different colours represent different *eta* values. Black horizontal dotted line represents the baseflow conditions where $\mu_\tau^* = 1$. Black solid curve corresponds to the shape of the hydrograph and gray line to the μ_τ^* for the reference scenario.

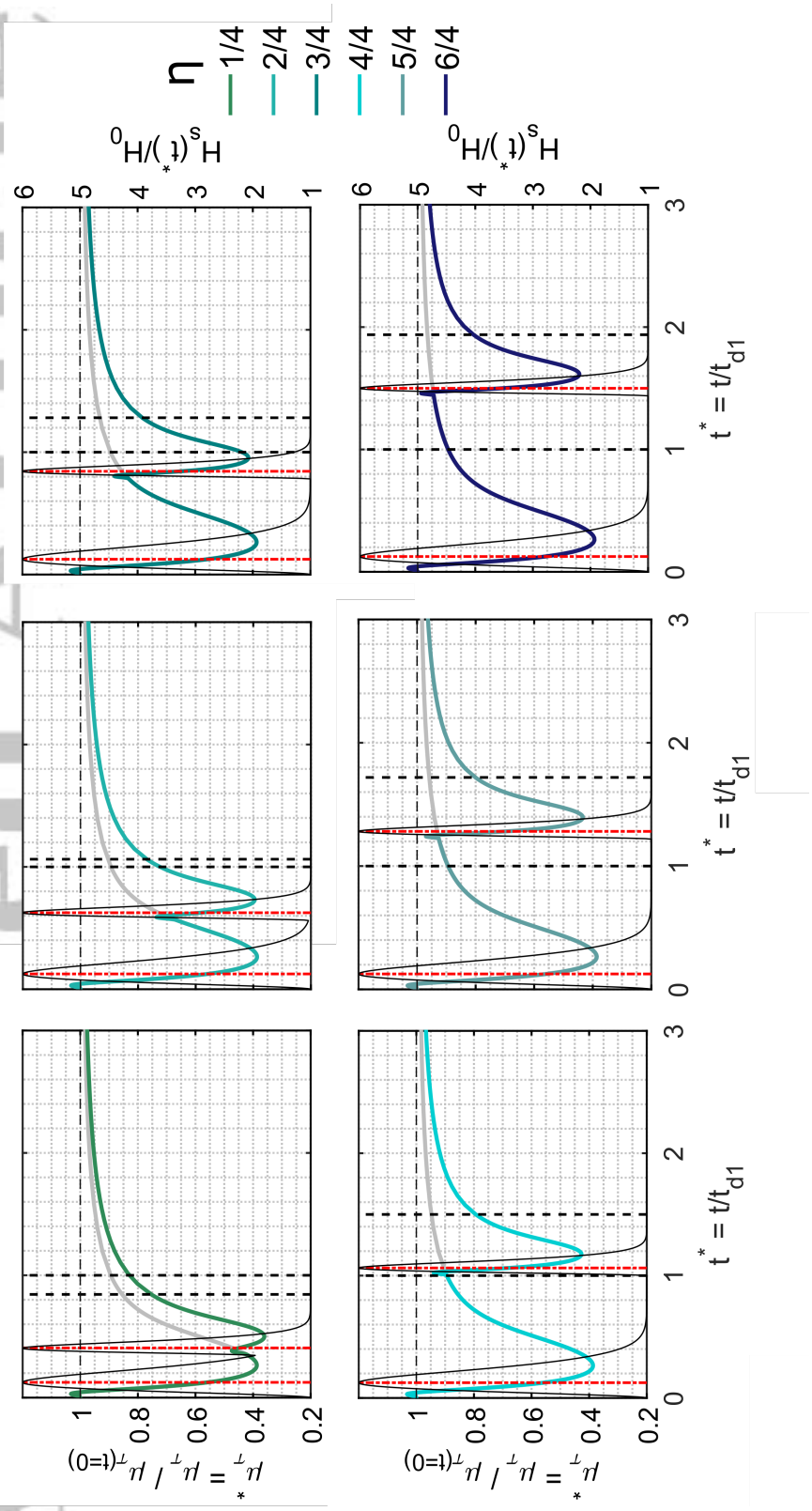

Figure 6. Temporal evolution of flux-weighted residence time μ_τ^* of hyporheic waters leaving the sediment-water interface, as a function of dimensionless time. Category 2 scenarios are shown where $H_{p1} = H_{p2}$ and $t_{d_1} > t_{d_2}$. Vertical red lines and black lines correspond to time-to-peak and duration of the events respectively. Different colours represents different *eta* values. Black horizontal dotted line represents the baseflow conditions where $\mu_\tau^* = 1$. Black solid curve correspond to the shape of the hydrograph and gray line to the μ_τ^* for the reference scenario.

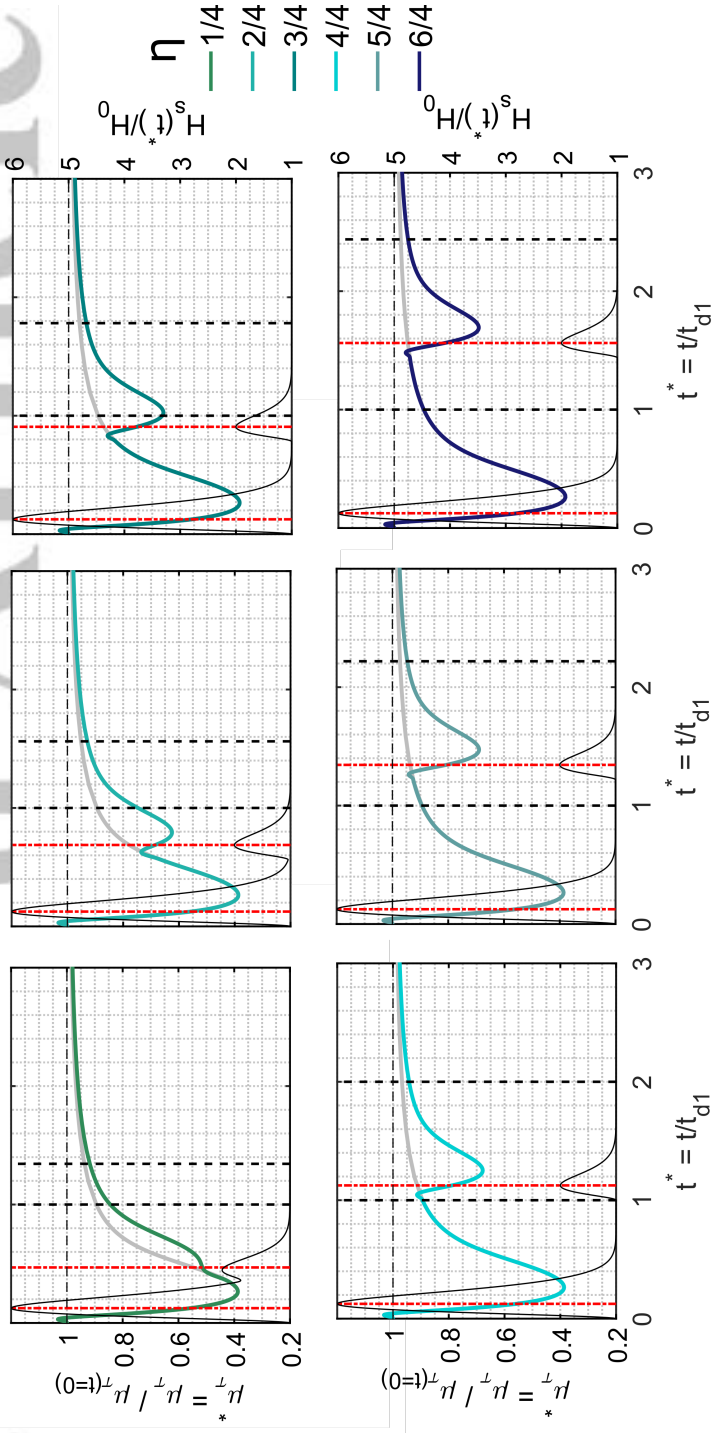

Figure 7. Temporal evolution of flux-weighted residence time μ_τ^* of hyporheic waters leaving the sediment-water interface, as a function of dimensionless time. Category 3 scenarios are shown where $H_{p_1} > H_{p_2}$ and $t_{d_1} = t_{d_2}$. Vertical red lines and black lines correspond to time-to-peak and duration of the events respectively. Different colours represents different *eta* values. Black horizontal dotted line represents the baseflow conditions where $\mu_\tau^* = 1$. The black solid curve corresponds to the shape of the hydrograph and gray line to the μ_τ^* for the reference scenario.

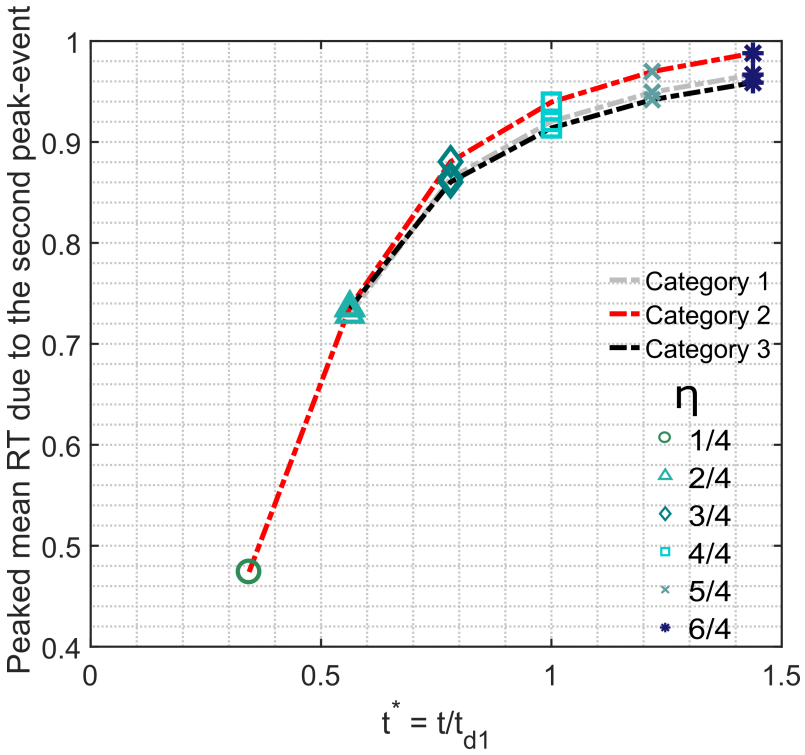

Figure 8. Peaked flux-weighted mean residence time of water leaving the hyporheic zone due to the second peak-flow event. Values are plotted as a function of time, *i.e.* the time when second (i.e. subsequent) peak-flow event commences (t_{lag}). Colours and symbols correspond to different values of η. Gray, red and black curves represent Category 1, 2 and 3 scenarios respectively.

conditions; see gray lines in Figures 5, 6 and 7) for a short duration which eventually starts declining shortly after the second peak is attained.

Variations in different scenarios is observed for different values of η. The results indicate that consecutively increasing the separation between the time-to-peak of the two events, t_{lag}, exhibits higher variability of μ_τ^* (increase in the difference between the troughs in mean residence time, that is, the variability in mean residence time from one event to the next). The hyporheic waters discharged from the sediment-water interface during successive peak-flow events is older, compared to the μ_τ^* for reference scenario (*i.e.* when the subsequent peak-flow event does not exist) for the scenarios with $\eta = 3/4, 4/4, 5/4$ and $6/4$. On the other hand, two events with a short interval of time in between causes lesser variability primarily because of activation of shorter subsurface flow paths with high flow velocities, leading to mixing of younger water in the hyporheic zone and decreasing μ_τ^*. Increased duration of the subsequent event deviates the system from the reference scenario for a longer period of time (Figures 5 and 7). Moreover, increased magnitude of the subsequent peak-flow event (i.e. when $H_{p_1} = H_{p_2}$; Figure 6) leads to discharge of younger hyporheic water into the channel (i.e., water with lower values of μ_τ^*) after the time-to-peak of the event, when compared to the scenarios with $H_{p_1} > H_{p_2}$ (Figures 5 and 7).

Further analysis of maxima of the first central moment of flux-weighted mean residence time for the second peak, μ_{max} shows interesting results (Figure 8). When two peak-flow events occur with shorter separation time (t_{lag}), mean age of the hyporheic waters leaving the streambed is relatively younger. Consecutively, increasing the value of t_{lag}, μ_{max} increases. When the η is 5/4 and 6/4, the maxima of central moment (μ_{max}) slowly reaches the plateau where for any further increase μ_{max} become constant. This is an indication that the two events become independent with no memory

effects from the antecedent peak-flow event is carried forward to the subsequent event and hence any response of the system is solely due to the subsequent event. Furthermore, subsequent peak-flow event with larger magnitude increased the peaked mean RT (μ_{max}) (red curve in Figure 8). Also note that for $\eta = 1/4$, scenarios associated with category 2 and 3 do not exhibit a μ_{max} (see black and gray curve in Figure 8, instead there is a slight deviations from attaining reference scenario conditions.

3.3 Numerical breakthrough curves

Conservative solute tracer retention was determined by estimating and comparing the integrated mass fluxes for different case-defined concentrations tracers. Mass entering and leaving the system was computed by multiplying the discharge by the concentration of conservative solute tracer entering the streambed and leaving the hyporheic zones (*i.e.* $C \geq 0.9C_s$) respectively. Breakthrough curves of tracers were determined by comparing the integrated mass fluxes leaving the system to the total mass injected.

Observations from the numerical tracer tests and its response to successive peak-flow events provided insights into the complex retention and transport behaviour of conservative solute tracers within a sediment domain. For the scenario with $\eta = 1/4$ in Figure 9, the breakthrough curve for c_1 is steeper, due to higher mass-transfer rate owing to shorter lag between the two events. As the concentration of c_2 emerges, the c_1 is pressed out of the hyporheic zones at a faster rate. c_2 tracer corresponds to the concentrations which is the combination or mixing of antecedent and the subsequent peak-flow events which exhibits broader breakthrough curve for $\eta = 1/4$. Another spike in c_1 indicates activation of the antecedent peak-flow event after cessation of the subsequent peak-flow event. Longest mass transfer, i.e. flatter breakthrough curve for the c_1 is observed for the scenarios with $\eta = 4/4, 5/4$ and $6/4$, primarily due to non-interference and non-superimposition of subsequent peak-flow event. Similar behavior is observed for the subsequent peak-flow event *i.e.* for c_3. Shape of the breakthrough curve is dependent on the flow rate and diffusion characteristics. When the lag between the two events is shorter, the solutes are relatively less retained in the system and transported at a faster rate, potentially from the shorter flow paths. In addition, it is also observed that as t_{lag} increases, the antecedent event's behaviour becomes similar to the reference concentration which represents the scenario with a single peak-flow event *i.e.* c_1 for $\eta = 6/4$ nearly coincided with reference concentration (black solid curve). Furthermore, increase in the magnitude of the subsequent peak-flow event causes the concentration to increase at a faster rate (see Figure 10).

A prominent observation in breakthrough curves for scenarios with longer duration of the subsequent event (Figure 11) is that the curves are much flatter when compared to scenarios with shorter duration. This can be explained by the slower mass transfer due to the longer spread of the event. Moreover, for $\eta = 1/4$, c_3 tracer is also injected as the longer duration of the subsequent event causes partial over lapping of the events and not complete as for the same condition in Category 1 scenario (Figure 9).

3.4 Solute transport retention and dynamics during the successive peak-flow events

Observations of the flux-weighted mean age and breakthrough curves unravelled interesting results detailing the impact of successive peak-flow events on water and solutes' residence times and transport. The increased transient pressure gradient due to the peak-flow events induces hyporheic flows that are primarily an instantaneous response to changes in the river stage. This instantaneous increase enlarges the size of hyporheic zones, elongates the subsurface flow paths and increases hyporheic fluxes. Sudden rises in stage induce newly activated deeper and elongated subsurface flow paths that increase the transport timescale for the water and solutes. The results indicated that the duration of the impact in the residence times caused by the antecedent event is highly determined by the flow characteristics of the subsequent peak-flow event. For example, if the subsequent peak-flow event with a shorter magnitude occurs immediately after the antecedent event, there is only minor deviation in the change in residence times. The intensity, time of occurrence and duration of the subsequent peak-flow event determine the magnitude of variations in the residence times over

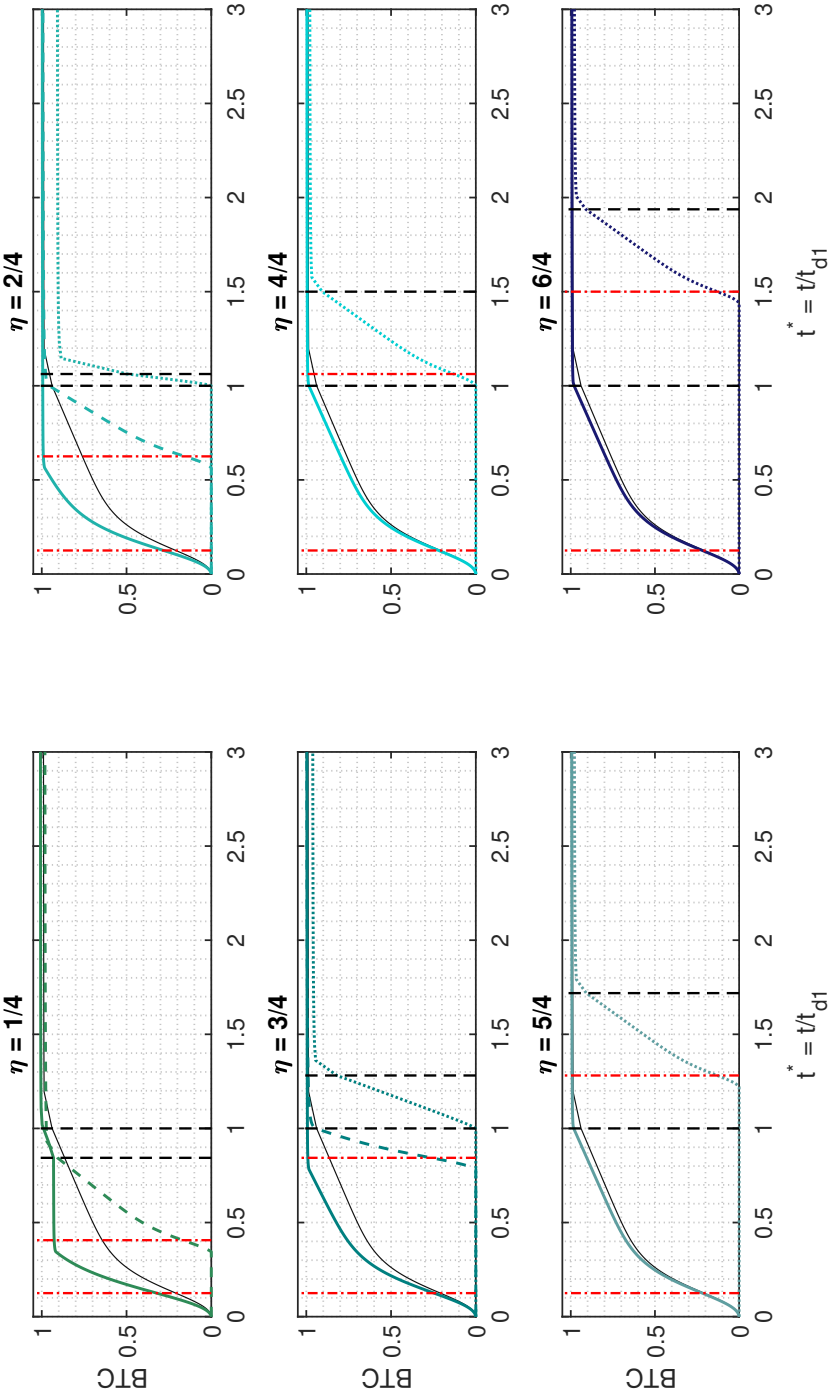

Figure 9. Modeled breakthrough curve as a function of dimensionless time. Category 1 scenarios are shown where $H_{p_1} > H_{p_2}$ and $t_{d_1} = t_{d_2}$. Solid coloured lines correspond to c_1 (i.e. when 1st event is active), dashed coloured lines for c_2 (i.e. when both the events are active at the same time) and dotted lines is for c_3 (i.e. when only 2nd event is active). Vertical red lines and black lines correspond to time-to-peak and duration of the events respectively. Gray line represents breakthrough curves for the reference scenario. Different colours represents different η values.

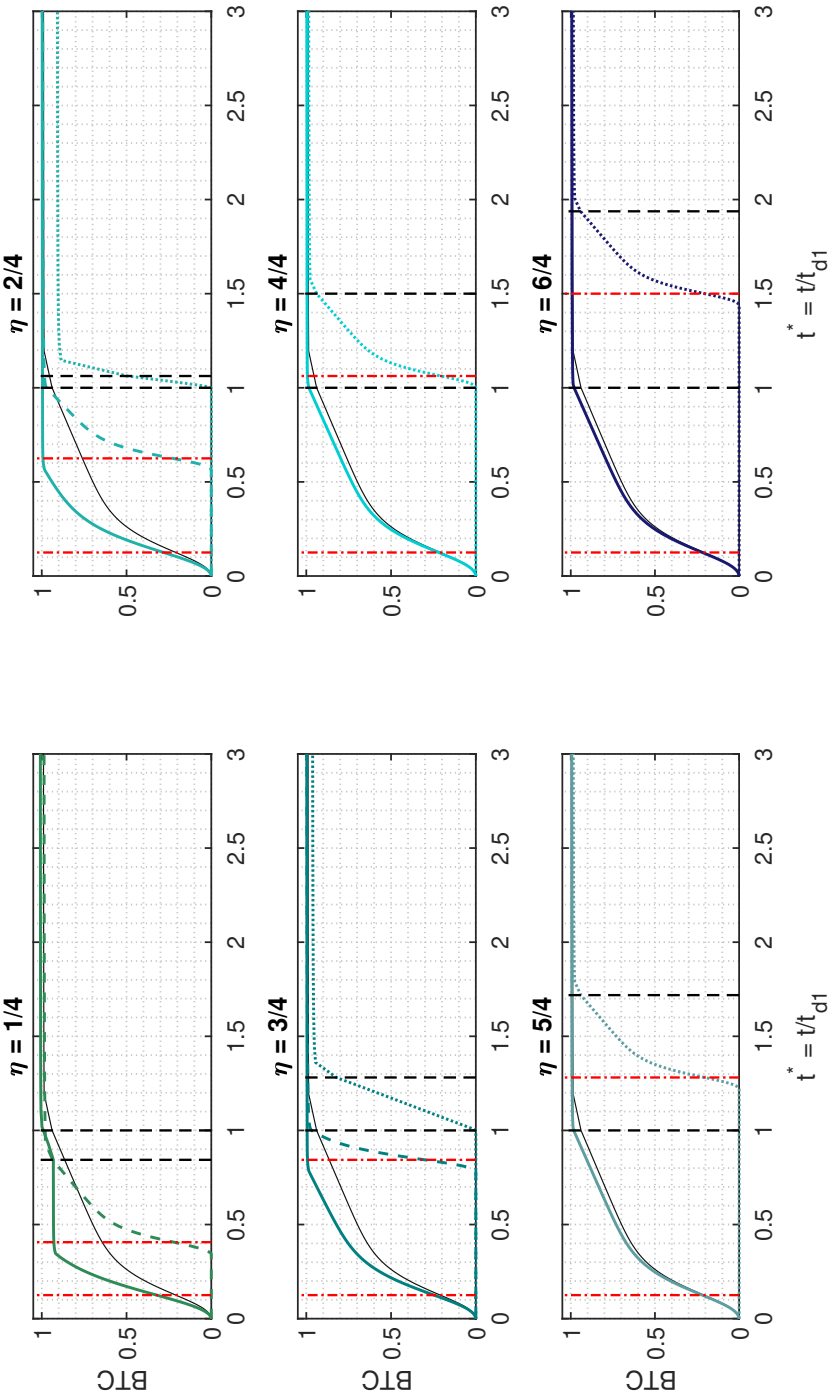

Figure 10. Modeled breakthrough curve as a function of dimensionless time. Category 1 scenarios are shown where $H_{p_1} = H_{p_2}$ and $t_{d_1} > t_{d_2}$. Solid coloured lines correspond to c_1 (i.e. when 1st event is active), dashed coloured lines for c_2 (i.e when both the events are active at the same time) and dotted lines is for c_3 (i.e. when only 2nd event is active). Vertical red lines and black lines correspond to time-to-peak and duration of the events respectively. Gray line represents breakthrough curves for the reference scenario. Different colours represents different η values.

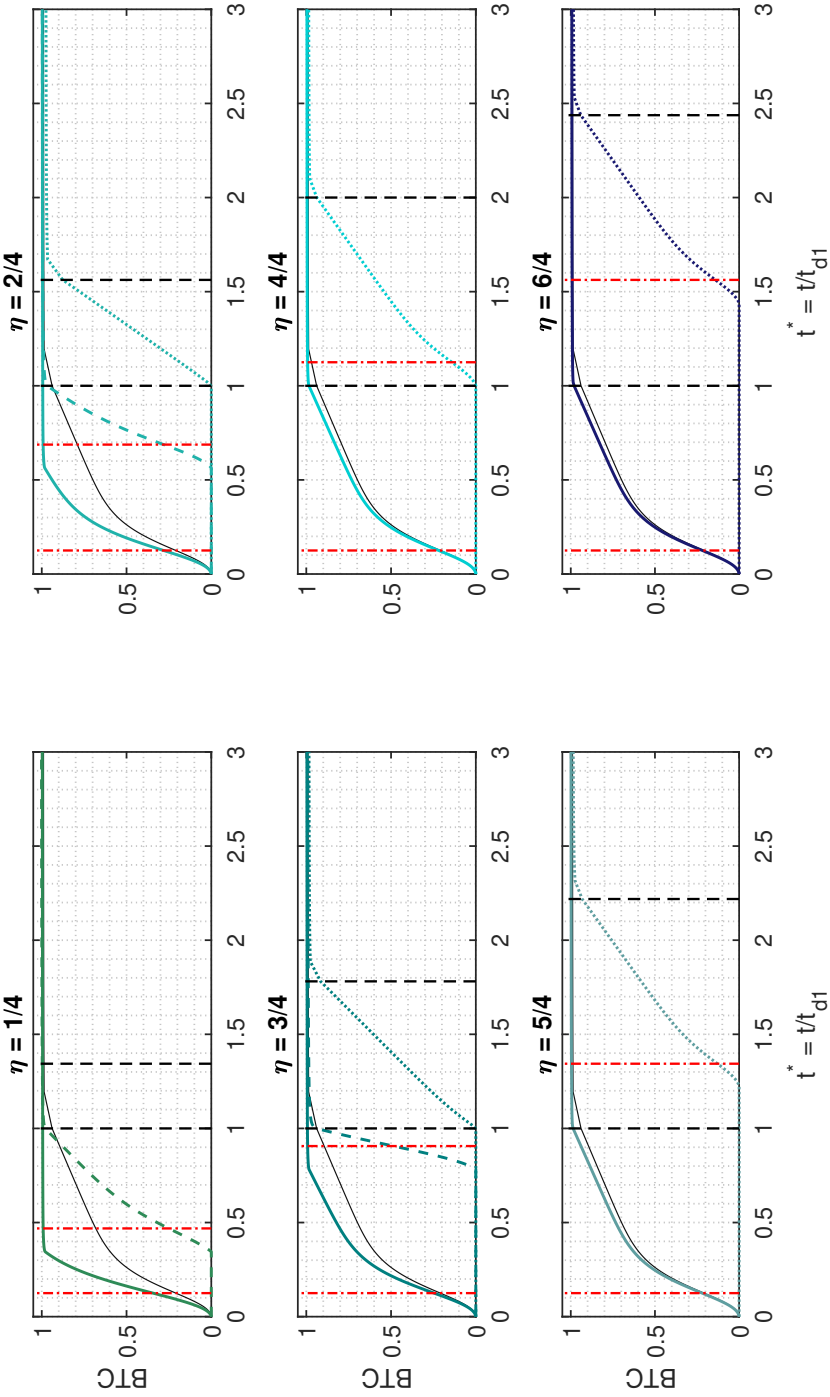

Figure 11. Modeled breakthrough curve as a function of dimensionless time. Category 1 scenarios are shown where $H_{p_1} > H_{p_2}$ and $t_{d_1} = t_{d_2}$. Solid coloured lines correspond to c_1 (i.e. when 1st event is active), dashed coloured lines for c_2 (i.e. when both the events are active at the same time) and dotted lines is for c_3 (i.e. when only 2nd event is active). Vertical red lines and black lines correspond to time-to-peak and duration of the events respectively. Gray line represents breakthrough curves for the reference scenario. Different colours represents different η values.

the course of events. Primarily, when the subsequent peak-flow event is of a large magnitude, the changes can be considerable and can exhibit long term change in the system. As also illustrated by Harvey et al. (2012), discharge with longer duration and larger magnitude will potentially completely flush deeper and longer flow paths.It can furthermore be useful to consider the modulating role of groundwater fluxes in tandem with the effects of sequential peak-flow events. The role of groundwater upwelling and downwelling has been documented in the study by Wu et al. (2018) for single peak-flow events, where the authors found that the regional groundwater flow and geomorphological settings greatly modulate the temporal evolution of bedform-induced hyporheic responses driven by a single peak-flow event. We expect that groundwater fluxes will have a similar modulating effect when a sequence of flood events is considered. For example, the subsequent event is likely to counteract the modulation of groundwater fluxes, changing the gradients adjacent to the streams, and hence reducing residence times and changing the patterns of solute transport. Future work will address this aspect in more detail.

Solute tracers results demonstrated that the peak-flow events can lead to prolonged storage and delayed release of solute tracers, for the scenarios where the two peak-flow events are not superimposed and occur for a longer duration of time. This is mainly because of the slower mass transfer due to the longer spread of the event. This is also indicated in the study by Harvey et al. (2012). Our results indicate that time-lag between two peak flow events (t_{lag}) is a crucial determinant of water and solutes retention time in the hyporheic zones. It is observed that if the time of the occurrence of the subsequent event is longer than the memory of the system from the antecedent event, the response of the successive events can be treated independently. However, other geomorphological parameters such as the channel gradient, bedform amplitude, wavelength (Elliott & Brooks, 1997; Singh et al., 2019; Wu et al., 2018) and flood characteristics like intensity, duration and skewness of the event also determine the transport and retention behaviour of water and solutes.

3.5 Biogeochemical and ecological implications

Herein we use numerical tracer tests to investigate the impacts of successive peak-flow events on water and solute retention and transport in sediment domain. This research mainly focuses on variations in hyporheic flux velocities, residence times and transport of conservative solutes under dynamic flow conditions. Our results indicate that high-flow events caused an expansion of the hyporheic zones and increase hyporheic fluxes, indicating that events have the potential to enhance down-welling of surface water rich in oxygen, dissolved organic matter, and other nutrients, being delivered into the hyporheic zone at high concentrations into greater depths and larger streambed areas (Gomez-Velez et al., 2017; Hester & Doyle, 2008; Singh et al., 2019). Findings by Drummond, Larsen, González-Pinzón, Packman, and Harvey (2017) suggested that storm events can mobilize or remobilize solutes and fine particles within the streambed and therefore further fuel biogeochemical transformations. That said, successive events occurring within a short duration of time *i.e.* when system is unable to recover from antecedent event may not enhance stream metabolism, owing to the larger amount of water pressed from shorter subsurface flow paths.

Sequential events have the potential to induce pockets with distinct chemical composition and steep reactive gradients within the hyporheic zone. For example, surface water solutes from the antecedent peak-flow event can be pushed at greater depths when the subsequent event commences. Then, a large proportion of the dissolved solutes from the subsequent event are flushed first through shorter and shallow subsurface flow paths while the solutes from the antecedent event remain within the streambed sediments. This mechanism can lead to biogeochemical *layering* and significantly affect the transport of dissolved organic carbon, dissolved oxygen, contaminants and microbes.

During successive peak-flow events, the altered hydraulic conditions affect the solute transport and retention. Increased residence times with longer separation between the two events suggests that high discharge events when occurred after a certain period of time has the potential to positively contribute to processes such as nitrification and denitrification. These results suggest that depending on the magnitude of the events, increased hyporheic flow paths due to repeated peak-flow events may enhance the stream metabolism. The results present by Trauth and Fleckenstein (2017) demon-

strated that a single discharge event increased the reactive efficiency of the hyporheic zone. Our findings highlight the effects of consecutive flow perturbations in the hydrodynamics and transport characteristics of the hyporheic exchange process. The compounding nature of these perturbations can have significant implications for the reactive efficiency of the hyporheic zone, and therefore, it should be considered in rivers exposed to natural and artificial (e.g., dam operations and waste-water discharge plants) fluctuation of flow As the biogeochemical timescales for oxygen consumption are important determinant for shifting the respiration from aerobic to anaerobic conditions in the streambed, elongated subsurface flow paths can promote biogeochemical transformations in deeper parts of the streambed (Gu, Hornberger, Herman, & Mills, 2008; Hinton et al., 1997; Inamdar et al., 2004; Kennedy, Genereux, Corbett, & Mitasova, 2009; Krause, Tecklenburg, Munz, & Naden, 2013; Malcolm et al., 2004). In addition, transience variability in hydraulic conditions and stream chemistry can have cascading influence on diversity and productivity of hyporheic organisms (Bruno et al., 2009).

4 Conclusions

Research results of this study highlight the relevance of considering the impacts of successive peak-flow events on hyporheic exchange flow, transport and retention times of water and conservative solutes within the streambed. Systematic hydrograph scenarios with variations in time-lag between the two flow events, magnitude and duration of the events were simulated with a two-dimensional model for sinusoidal bedforms and analyzed for flow, transport and residence time distributions. The time-lags between simulated event scenarios ranged from complete overlapping *i.e.* superimposition of two events, partial overlapping to scenarios with no overlapping *i.e.* representing repeated peak-flow events.

During peak-flow events, instantaneous changes in the temporally variable hyporheic flow field were observed due to rapid pressure wave propagation within the streambed. However, the actual increase in hyporheic flow as defined based on the geochemical definition of hyporheic zone reacted generally less sudden. The results demonstrate that longer time lags between successive peak-flow events cause higher temporal variability in the flux-weighted mean residence times, with a higher potential to discharge older hyporheic pore water compared to the reference scenario. Furthermore, with increasing time lag between two flow events, the maxima of the first central moment *i.e.* mean age slowly reaches the plateau where for any further increase, the value remains constant. Simulated breakthrough curves depicted generally reduced gradient for scenarios with longer time lags between events and enhanced duration of the subsequent event. Variability in event magnitude also had an impact on the shape of the breakthrough curves. Higher magnitude of the subsequent event caused the breakthrough curves to become steeper, when compared to low magnitude and longer duration of the subsequent event. It is observed that successive events can be treated independently if the occurrence of subsequent event is longer than the memory of the system from the antecedent event. The model-based analysis of simulated breakthrough curves of conservative tracer for successive peak-flow events highlights the impact of the type and duration of peak-flow successions on residence time distributions and solute transport that are relevant for biogeochemical turnover in hyporheic zones.

Acknowledgments

This project received the funding from the European Union's Horizon 2020 research and innovation programme under Marie Sklodowska-Curie grant agreement No. 641939 (HypoTRAIN) and No. 734317 (HiFreq). The work was partly supported by the German Research Foundation under the grant WO671/11-1. J.D. Gomez-Velez is funded by the U.S. National Science Foundation (award EAR 1830172) and the U.S. Department of Energy, Office of Biological and Environmental Research (BER), as part of BER's Subsurface Biogeochemistry Research Program (SBR). This contribution originates from the SBR Scientific Focus Area (SFA) at the Pacific Northwest National Laboratory (PNNL). All data required to reproduce the figures in this paper is available on the data repository of the University of Birmingham's library.

References

Bear, J. (1972). *Dynamics of fluids in porous media*. New York: American Elsevier Publishing.

Bernard-Jannin, L., Brito, D., Sun, X., Jauch, E., Neves, R., Sauvage, S., & Sánchez-Pérez, J.-M. (2016). Spatially distributed modelling of surface water-groundwater exchanges during overbank flood events–a case study at the garonne river. *Advances in water resources*, *94*, 146–159.

Boano, F., Revelli, R., & Ridolfi, L. (2013). Modeling hyporheic exchange with unsteady stream discharge and bedform dynamics. *Water Resources Research*, *49*(7), 4089–4099.

Bruno, M. C., Maiolini, B., Carolli, M., & Silveri, L. (2009). Impact of hydropeaking on hyporheic invertebrates in an alpine stream (trentino, italy). In *Annales de limnologie-international journal of limnology* (Vol. 45, pp. 157–170).

Cooper, H. H., & Rorabaugh, M. I. (1963). *Ground-water movements and bank storage due to flood stages in surface streams* (Ground Water Hydraulics No. Water Supply Paper 1536-J). US Geological Survey.

Dingman, S. L. (2009). *Fluvial Hydraulics*. Oxford ; New York: Oxford University Press, USA.

Drummond, J. D., Larsen, L. G., González-Pinzón, R., Packman, A. I., & Harvey, J. W. (2017). Fine particle retention within stream storage areas at base flow and in response to a storm event. *Water Resources Research*, *53*(7), 5690–5705.

Dudley-Southern, M., & Binley, A. (2015). Temporal responses of groundwater-surface water exchange to successive storm events. *Water Resources Research*, *51*(2), 1112–1126.

Elliott, A. H., & Brooks, N. H. (1997). Transfer of nonsorbing solutes to a streambed with bed forms: Theory. *Water Resources Research*, *33*(1), 123–136.

Fritz, B. G., & Arntzen, E. V. (2007). Effect of rapidly changing river stage on uranium flux through the hyporheic zone. *Groundwater*, *45*(6), 753–760.

Gomez-Velez, J. D., & Harvey, J. W. (2014). A hydrogeomorphic river network model predicts where and why hyporheic exchange is important in large basins. *Geophysical Research Letters*, *41*(18), 6403–6412.

Gomez-Velez, J. D., Krause, S., & Wilson, J. L. (2014). Effect of low-permeability layers on spatial patterns of hyporheic exchange and groundwater upwelling. *Water Resources Research*, *50*(6), 5196–5215.

Gomez-Velez, J. D., & Wilson, J. L. (2013). Age distributions and dynamically changing hydrologic systems: Exploring topography-driven flow. *Water Resources Research*, *49*(3), 1503–1522.

Gomez-Velez, J. D., Wilson, J. L., & Cardenas, M. B. (2012). Residence time distributions in sinuosity-driven hyporheic zones and their biogeochemical effects. *Water Resources Research*, *48*(9).

Gomez-Velez, J. D., Wilson, J. L., Cardenas, M. B., & Harvey, J. W. (2017). Flow and residence times of dynamic river bank storage and sinuosity-driven hyporheic exchange. *Accepted for publication in Water Resources Research*.

Gu, C., Hornberger, G. M., Herman, J. S., & Mills, A. L. (2008). Effect of freshets on the flux of groundwater nitrate through streambed sediments. *Water resources research*, *44*(5).

Harvey, J. W., Drummond, J. D., Martin, R. L., McPhillips, L. E., Packman, A. I., Jerolmack, D. J., ... Tobias, C. R. (2012). Hydrogeomorphology of the hyporheic zone: Stream solute and fine particle interactions with a dynamic streambed. *Journal of Geophysical Research: Biogeosciences*, *117*(G4).

Hester, E. T., & Doyle, M. W. (2008). In-stream geomorphic structures as drivers of hyporheic exchange. *Water Resources Research*, *44*(3).

Hinton, M. J., Schiff, S. L., & English, M. C. (1997). The significance of storms for the concentration and export of dissolved organic carbon from two precambrian shield catchments. *Biogeochemistry*, *36*(1), 67–88.

Inamdar, S. P., Christopher, S. F., & Mitchell, M. J. (2004). Export mechanisms for dissolved organic carbon and nitrate during summer storm events in a glaciated forested catchment in new york, usa. *Hydrological Processes*, *18*(14), 2651–2661.

Jiang, X.-W., Wang, X.-S., Wan, L., & Ge, S. (2011). An analytical study on stagnation points in nested flow systems in basins with depth-decaying hydraulic conductivity. *Water Resources Research*, *47*(1).

Kennedy, C. D., Genereux, D. P., Corbett, D. R., & Mitasova, H. (2009). Spatial and temporal dynamics of coupled groundwater and nitrogen fluxes through a streambed in an agricultural watershed. *Water Resources Research*, *45*(9).

Krause, S., Boano, F., Cuthbert, M. O., Fleckenstein, J. H., & Lewandowski, J. (2014). Understanding process dynamics at aquifer-surface water interfaces: An introduction to the special section on new modeling approaches and novel experimental technologies. *Water Resources Research*, *50*(2), 1847–1855.

Krause, S., & Bronstert, A. (2007). Water balance simulations and groundwater—surface water interactions in a mesoscale lowland river catchment. *Hydrological Processes*, *21*, 169–184.

Krause, S., Hannah, D. M., Fleckenstein, J. H., Heppell, C. M., Kaeser, D., Pickup, R., ... Wood, P. J. (2011). Inter-disciplinary perspectives on processes in the hyporheic zone. *Ecohydrology*, *4*(4), 481–499.

Krause, S., Tecklenburg, C., Munz, M., & Naden, E. (2013). Streambed nitrogen cycling beyond the hyporheic zone: Flow controls on horizontal patterns and depth distribution of nitrate and dissolved oxygen in the upwelling groundwater of a lowland river. *Journal of Geophysical Research: Biogeosciences*, *118*(1), 54–67.

Liang, X., Zhan, H., & Schilling, K. (2018). Spatiotemporal responses of groundwater flow and aquifer-river exchanges to flood events. *Water Resources Research*, *54*(3), 1513–1532.

Lotts, W. S., & Hester, E. T. (2020). Filling the void: the effect of streambank soil pipes on transient hyporheic exchange during a peak flow event. *Water Resources Research*, *56*.

Malcolm, I. A., Soulsby, C., Youngson, A. F., Hannah, D. M., McLaren, I. S., & Thorne, A. (2004). Hydrological influences on hyporheic water quality: implications for salmon egg survival. *Hydrological Processes*, *18*(9), 1543–1560.

Malzone, J. M., Anseeuw, S. K., Lowry, C. S., & Allen-King, R. (2016, March). Temporal Hyporheic Zone Response to Water Table Fluctuations. *Groundwater*, *54*(2), 274–285.

Malzone, J. M., Lowry, C. S., & Ward, A. S. (2016, June). Response of the hyporheic zone to transient groundwater fluctuations on the annual and storm event time scales. *Water Resources Research*.

Marzadri, A., Tonina, D., Bellin, A., & Valli, A. (2016). Mixing interfaces, fluxes, residence times and redox conditions of the hyporheic zones induced by dune-like bedforms and ambient groundwater flow. *Advances in Water Resources*, *88*, 139–151.

McCallum, J. L., & Shanafield, M. (2016). Residence times of stream-groundwater exchanges due to transient stream stage fluctuations. *Water Resources Research*.

Menichino, G. T., & Hester, E. T. (2015). The effect of macropores on bi-directional hydrologic exchange between a stream channel and riparian groundwater. *Journal of Hydrology*, *529*, 830–842.

Millington, R. J., & Quirk, J. P. (1961). Permeability of porous solids. *Transactions of the Faraday Society*, *57*, 1200–1207.

Mojarrad, B. B., Betterle, A., Singh, T., Olid, C., & Wörman, A. (2019). The effect of stream discharge on hyporheic exchange. *Water*, *11*(7), 1436.

Munz, M., Krause, S., Tecklenburg, C., & Binley, A. (2011). Reducing monitoring gaps at the aquifer–river interface by modelling groundwater–surface water exchange flow patterns. *Hydrological Processes*, *25*(23), 3547–3562.

Pinay, G., Peiffer, S., De Dreuzy, J.-R., Krause, S., Hannah, D. M., Fleckenstein, J. H., ... Hubert-Moy, L. (2015). Upscaling nitrogen removal capacity from local hotspots to low stream orders' drainage basins. *Ecosystems*, *18*(6), 1101–1120.

Salazar, O., Vargas, J., Nájera, F., Seguel, O., & Casanova, M. (2014). Monitoring of nitrate leaching during flush flooding events in a coarse-textured floodplain soil. *Agricultural Water Management*, *146*, 218–227.

Sawyer, A. H., Cardenas, M. B., Bomar, A., & Mackey, M. (2009). Impact of dam operations on hyporheic exchange in the riparian zone of a regulated river. *Hydrological Processes: An International Journal*, *23*(15), 2129–2137.

Schmadel, N. M., Ward, A. S., Lowry, C. S., & Malzone, J. M. (2016). Hyporheic exchange controlled by dynamic hydrologic boundary conditions. *Geophysical Research Letters*, 2016GL068286.

Singh, T., Wu, L., Gomez-Velez, J. D., Lewandowski, J., Hannah, D. M., & Krause, S. (2019). Dy-

namic hyporheic zones: Exploring the role of peak flow events on bedform-induced hyporheic exchange. *Water Resources Research*, *55*(1), 218–235.

Stonedahl, S. H., Harvey, J. W., Wörman, A., Salehin, M., & Packman, A. I. (2010). A multiscale model for integrating hyporheic exchange from ripples to meanders. *Water Resources Research*, *46*(12).

Tonina, D., & Buffington, J. M. (2011). Effects of stream discharge, alluvial depth and bar amplitude on hyporheic flow in pool-riffle channels. *Water Resources Research*, *47*(8).

Trauth, N., & Fleckenstein, J. H. (2017). Single discharge events increase reactive efficiency of the hyporheic zone. *Water Resources Research*, *53*(1), 779–798.

Triska, F. J., Kennedy, V. C., Avanzino, R. J., Zellweger, G. W., & Bencala, K. E. (1989). Retention and transport of nutrients in a third-order stream in northwestern california: hyporheic processes. *Ecology*, 1893–1905.

Vivoni, E. R., Bowman, R. S., Wyckoff, R. L., Jakubowski, R. T., & Richards, K. E. (2006). Analysis of a monsoon flood event in an ephemeral tributary and its downstream hydrologic effects. *Water Resources Research*, *42*(3).

Ward, A. S., Gooseff, M. N., Voltz, T. J., Fitzgerald, M., Singha, K., & Zarnetske, J. P. (2013). How does rapidly changing discharge during storm events affect transient storage and channel water balance in a headwater mountain stream? *Water Resources Research*, *49*(9), 5473–5486.

Ward, A. S., Schmadel, N. M., & Wondzell, S. M. (2018). Time-variable transit time distributions in the hyporheic zone of a headwater mountain stream. *Water Resources Research*, *54*(3), 2017–2036.

Wörman, A., Packman, A. I., Marklund, L., Harvey, J. W., & Stone, S. H. (2006). Exact three-dimensional spectral solution to surface-groundwater interactions with arbitrary surface topography. *Geophysical Research Letters*, *33*(7).

Wu, L., Singh, T., Gomez-Velez, J. D., Nützmann, G., Wörman, A., Krause, S., & Lewandowski, J. (2018). Impact of dynamically changing discharge on hyporheic exchange processes under gaining and losing groundwater conditions. *Water Resources Research*, *54*(12), 10–076.

Zarnetske, J. P., Haggerty, R., Wondzell, S. M., & Baker, M. A. (2011). Dynamics of nitrate production and removal as a function of residence time in the hyporheic zone. *Journal of Geophysical Research: Biogeosciences*, *116*(G1).

Figure 1.

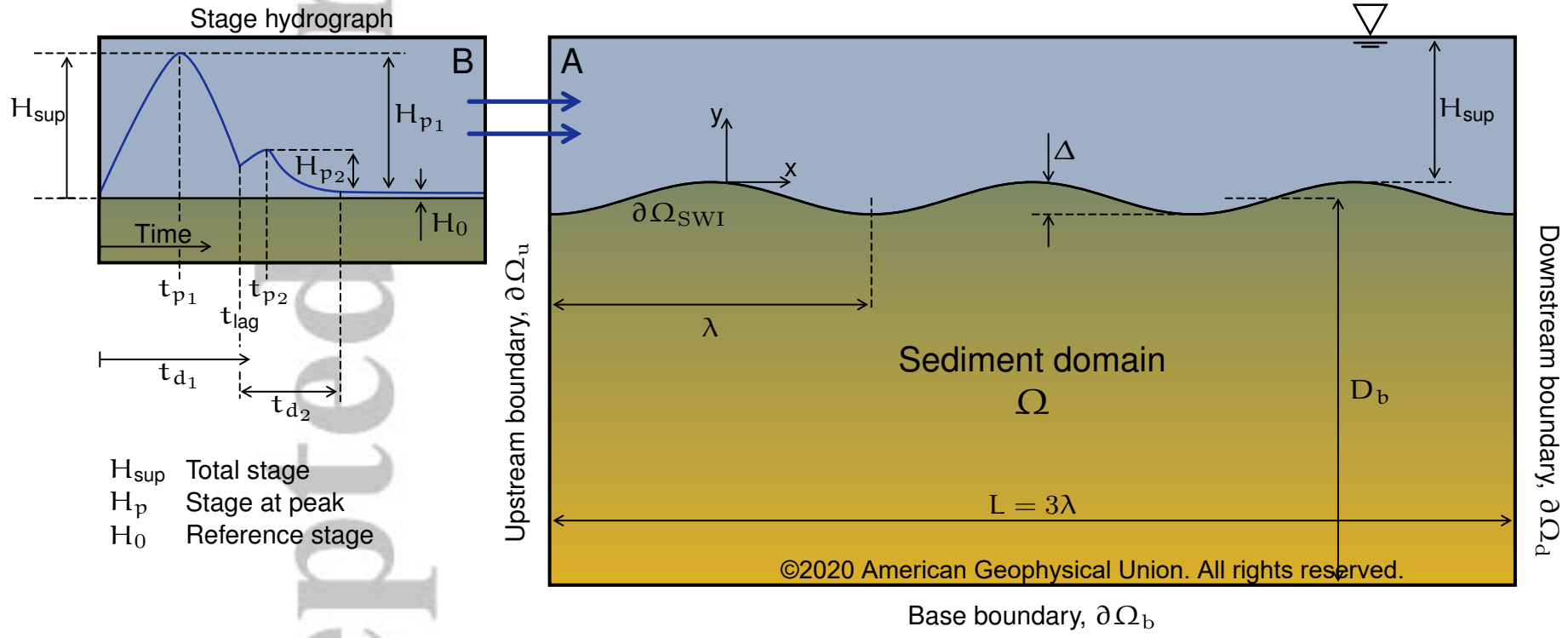

Figure 2.

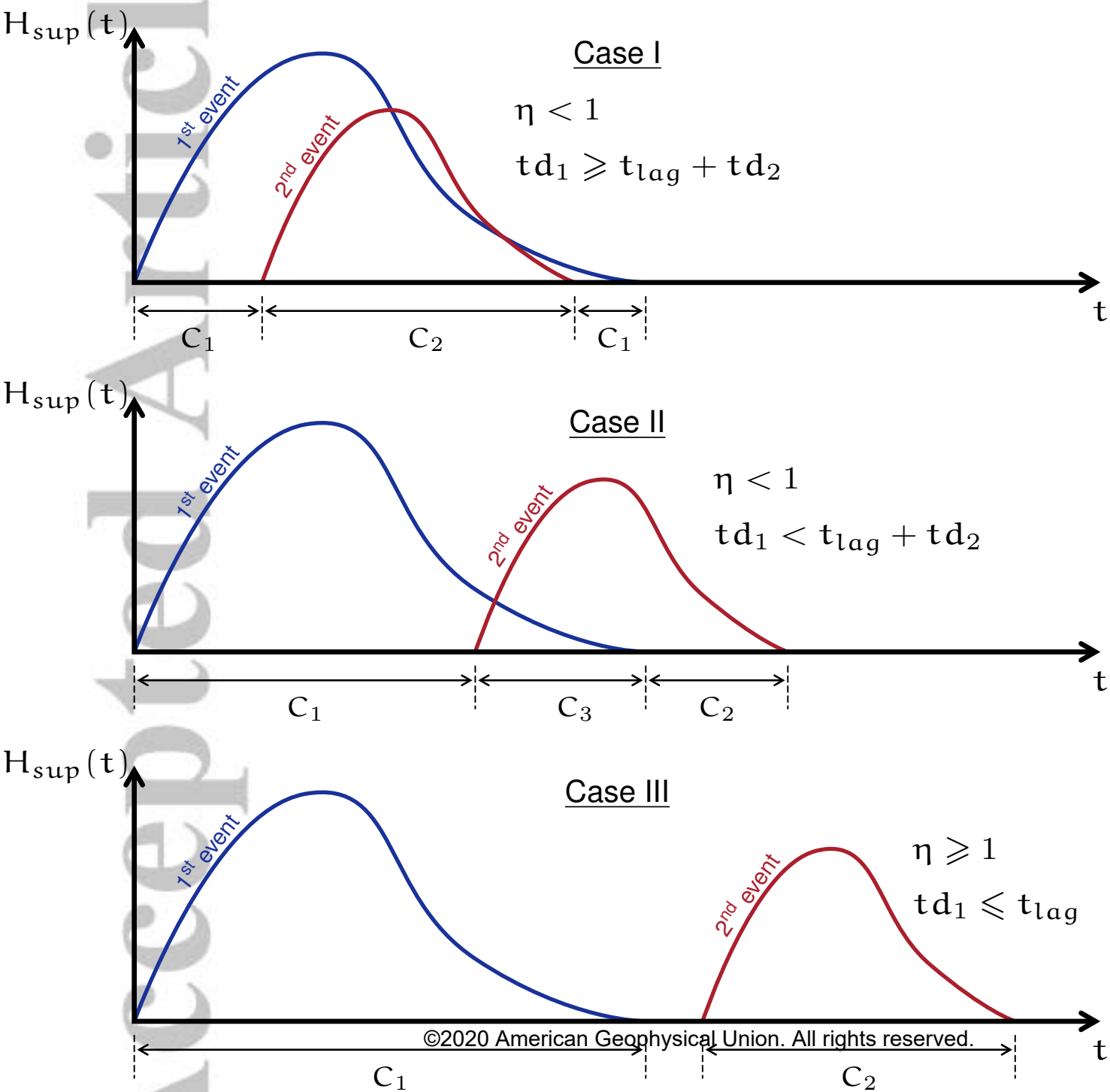

Figure 3.

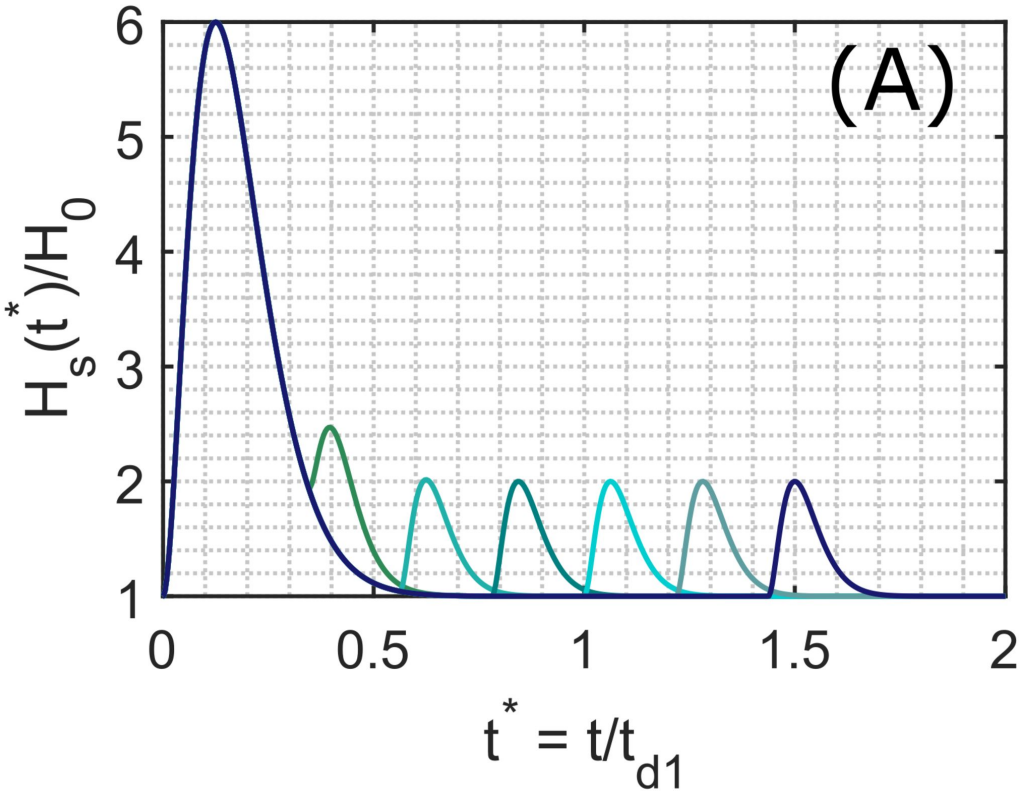

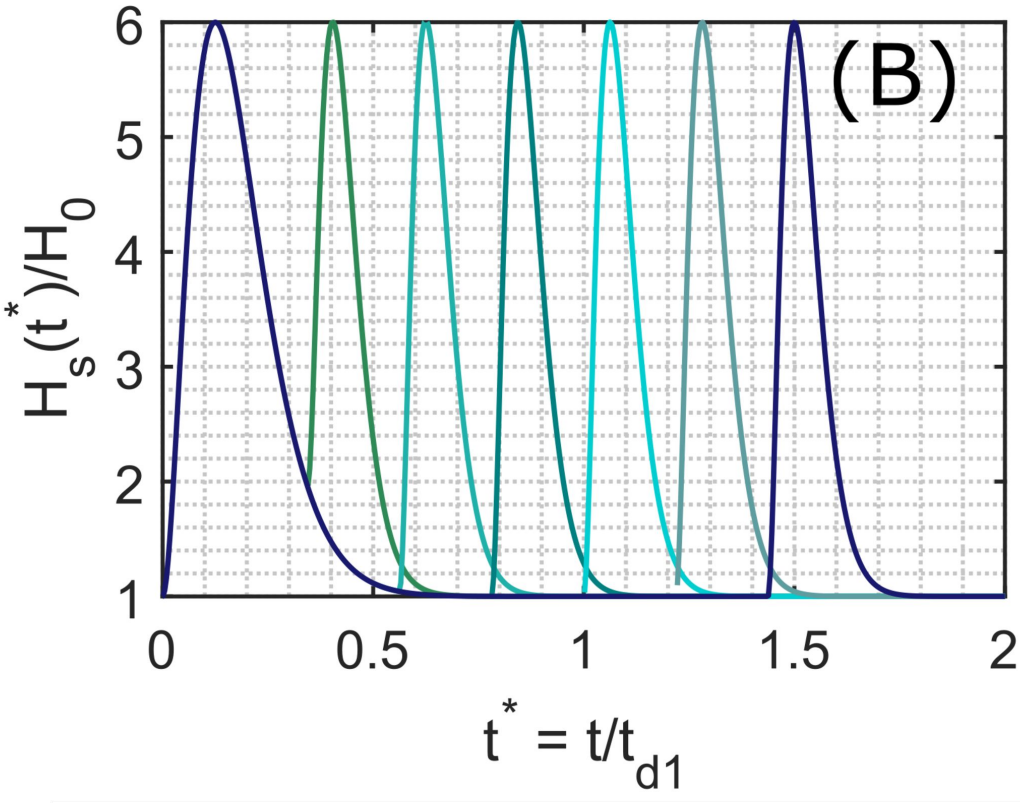

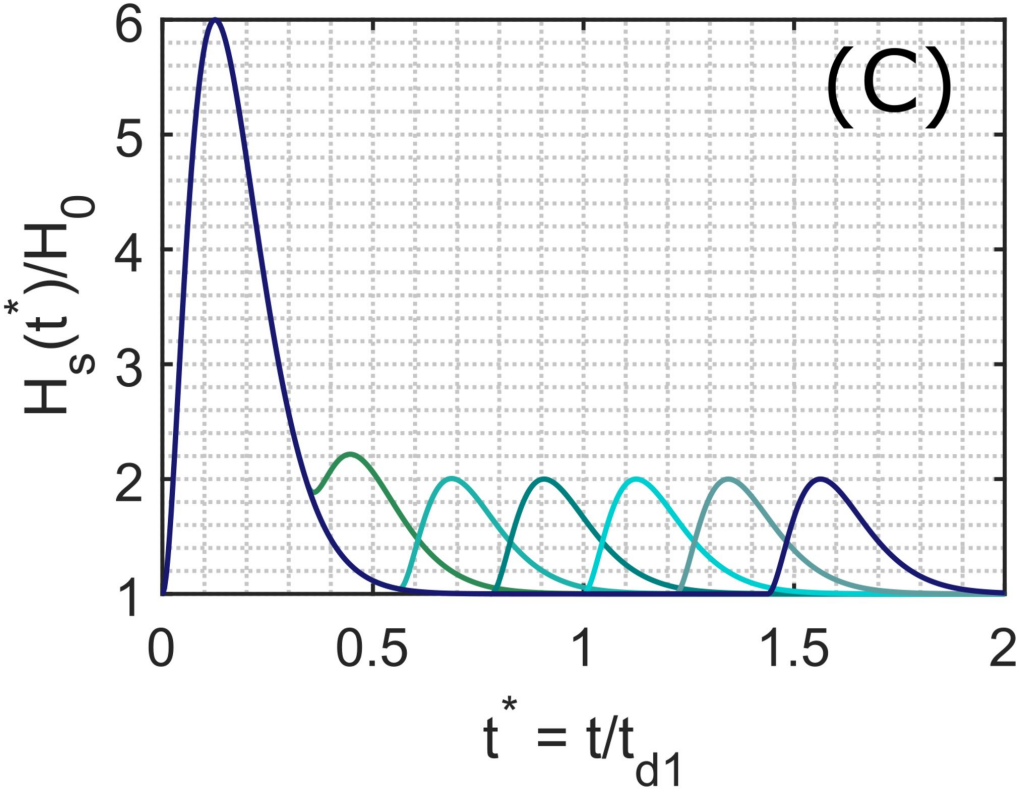

Figure 4.

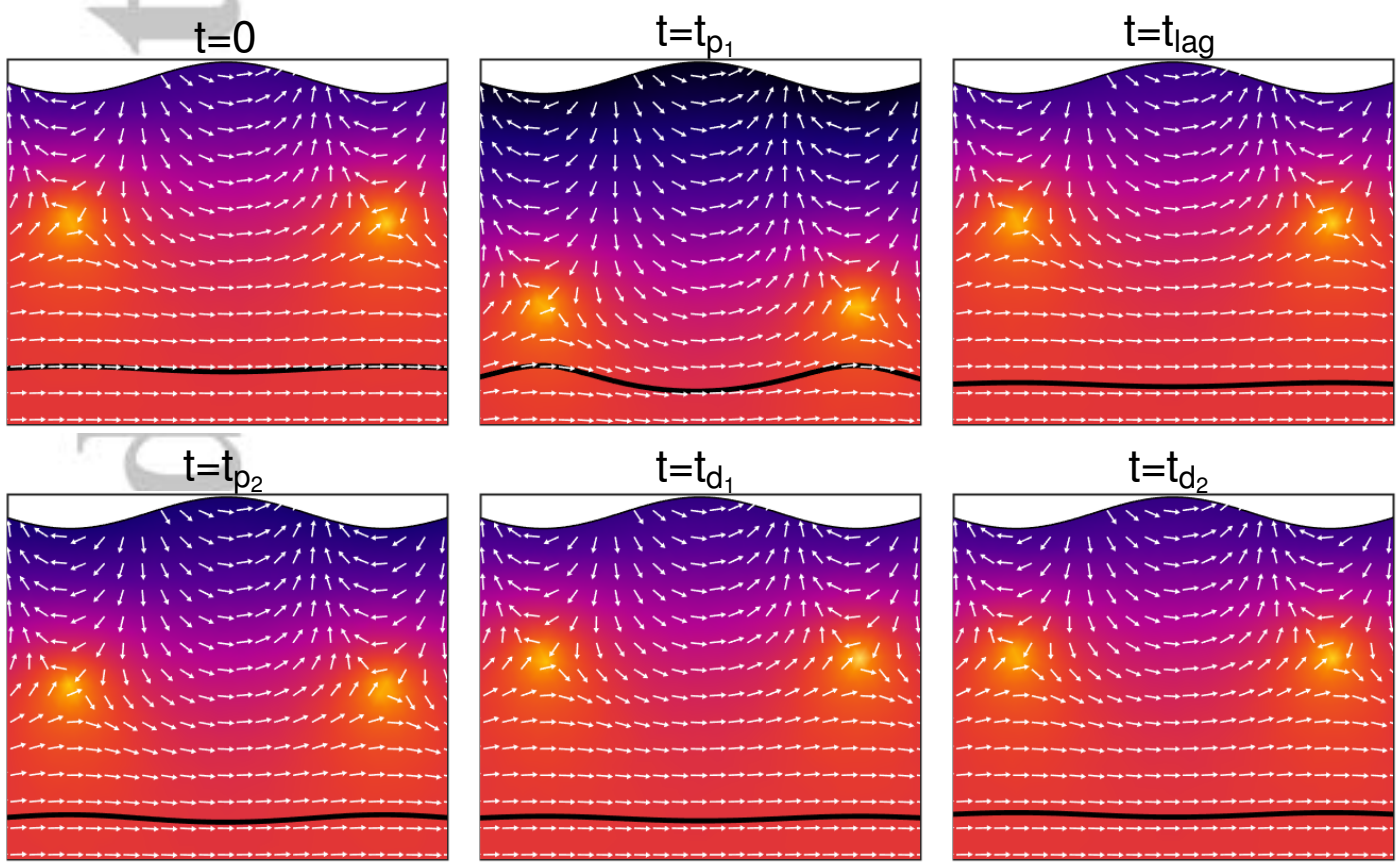

Figure 5.

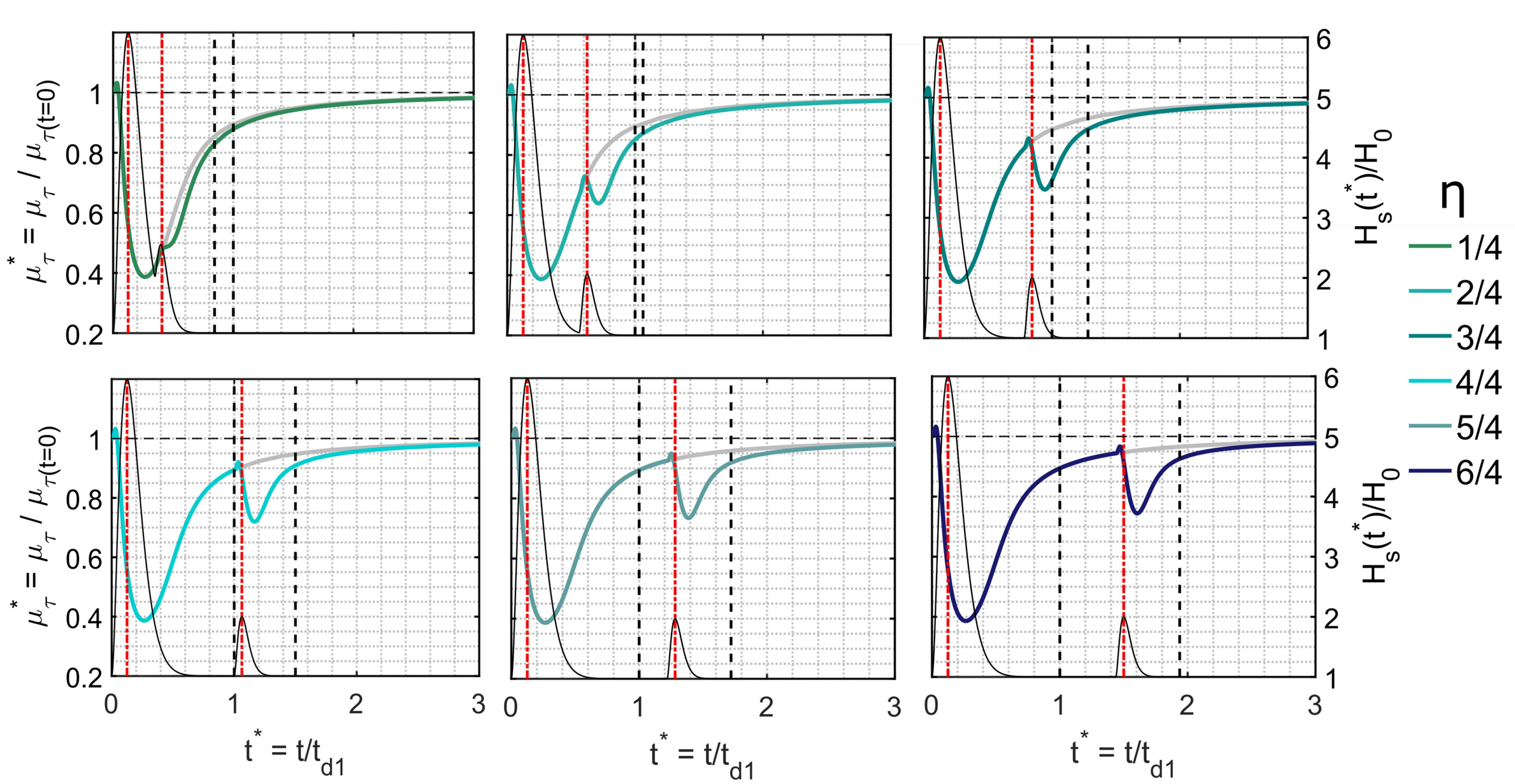

Figure 6.

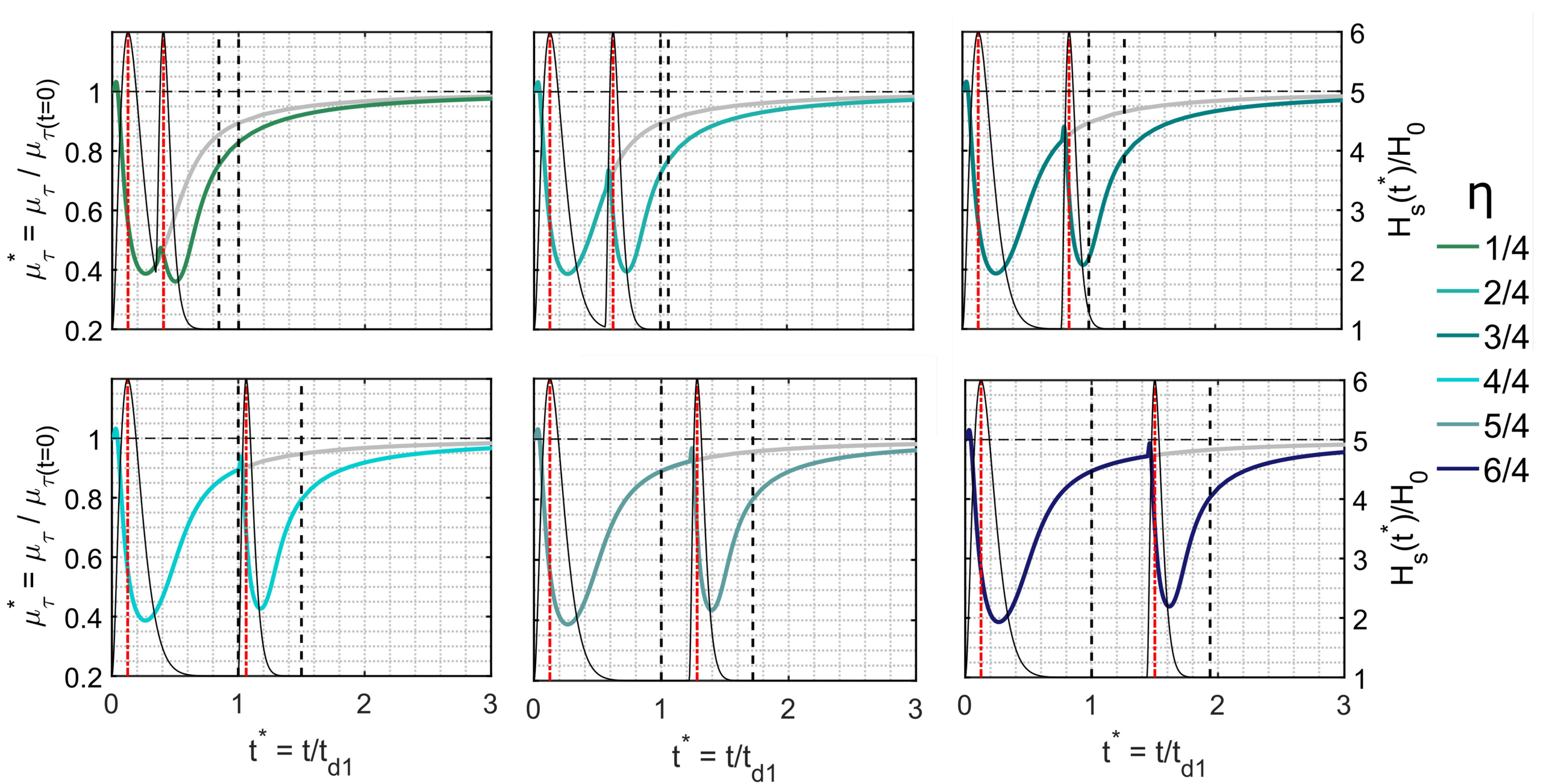

Figure 7.

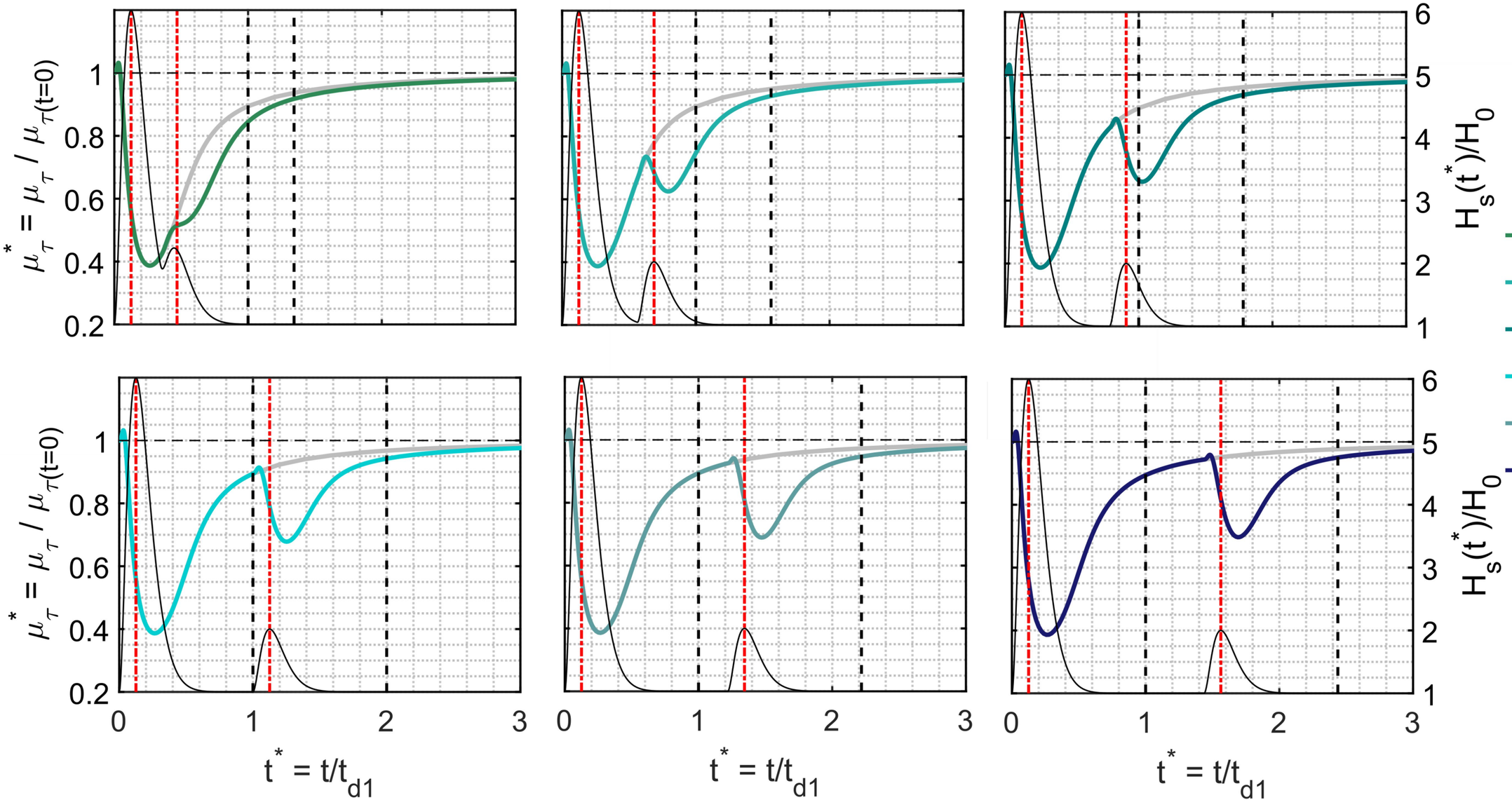

Figure 8.

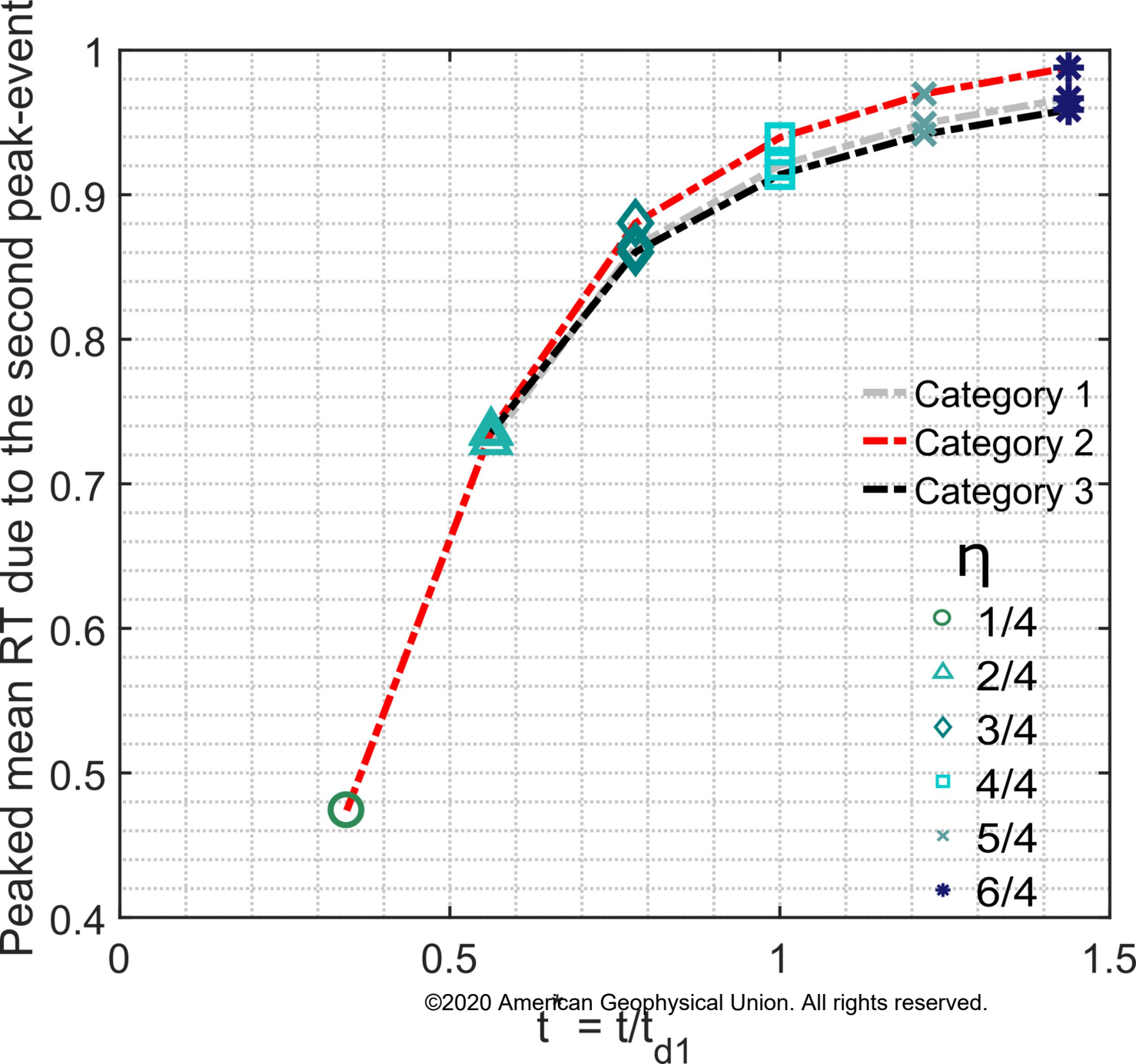

Figure 9.

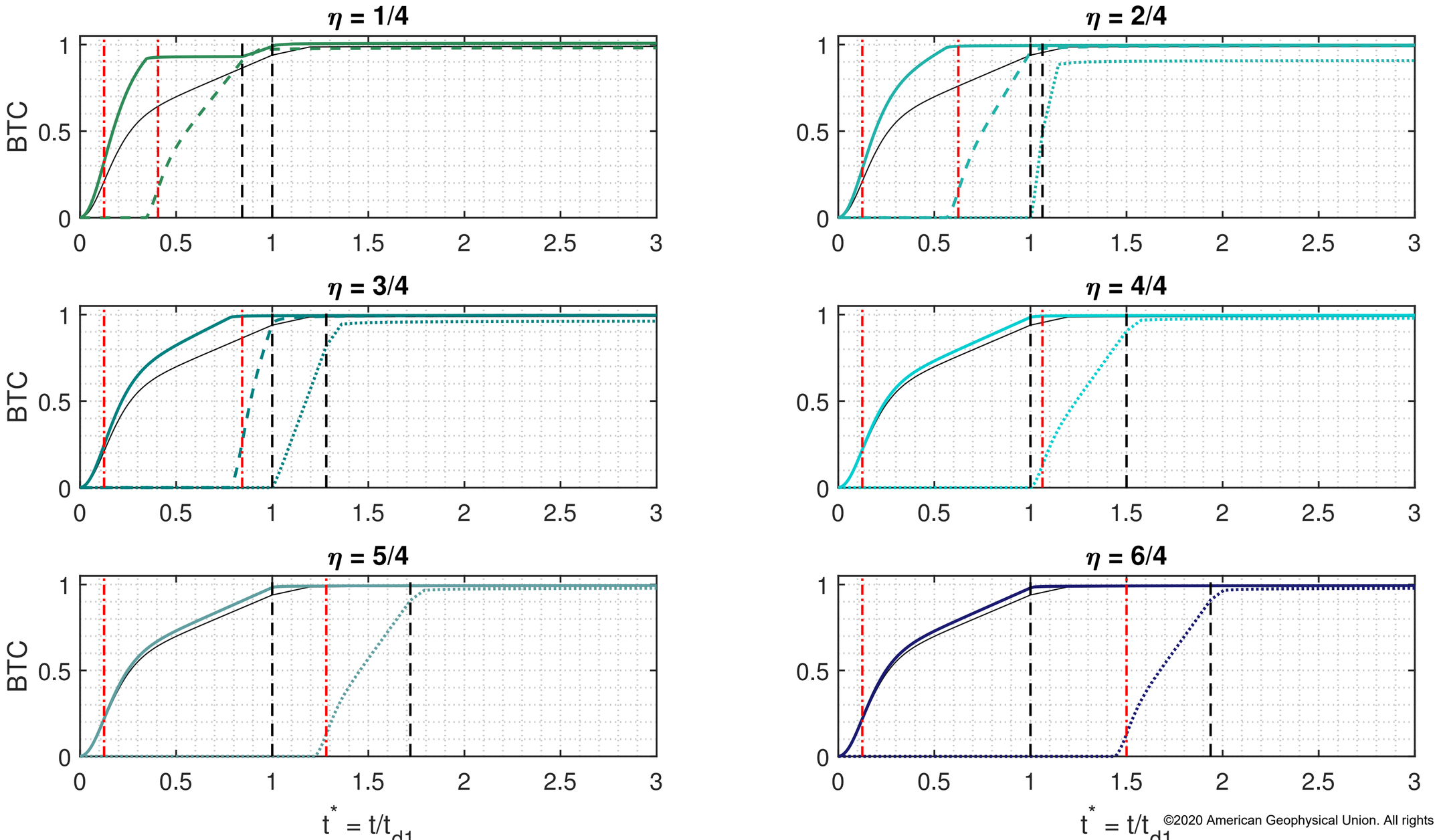

Figure 10.

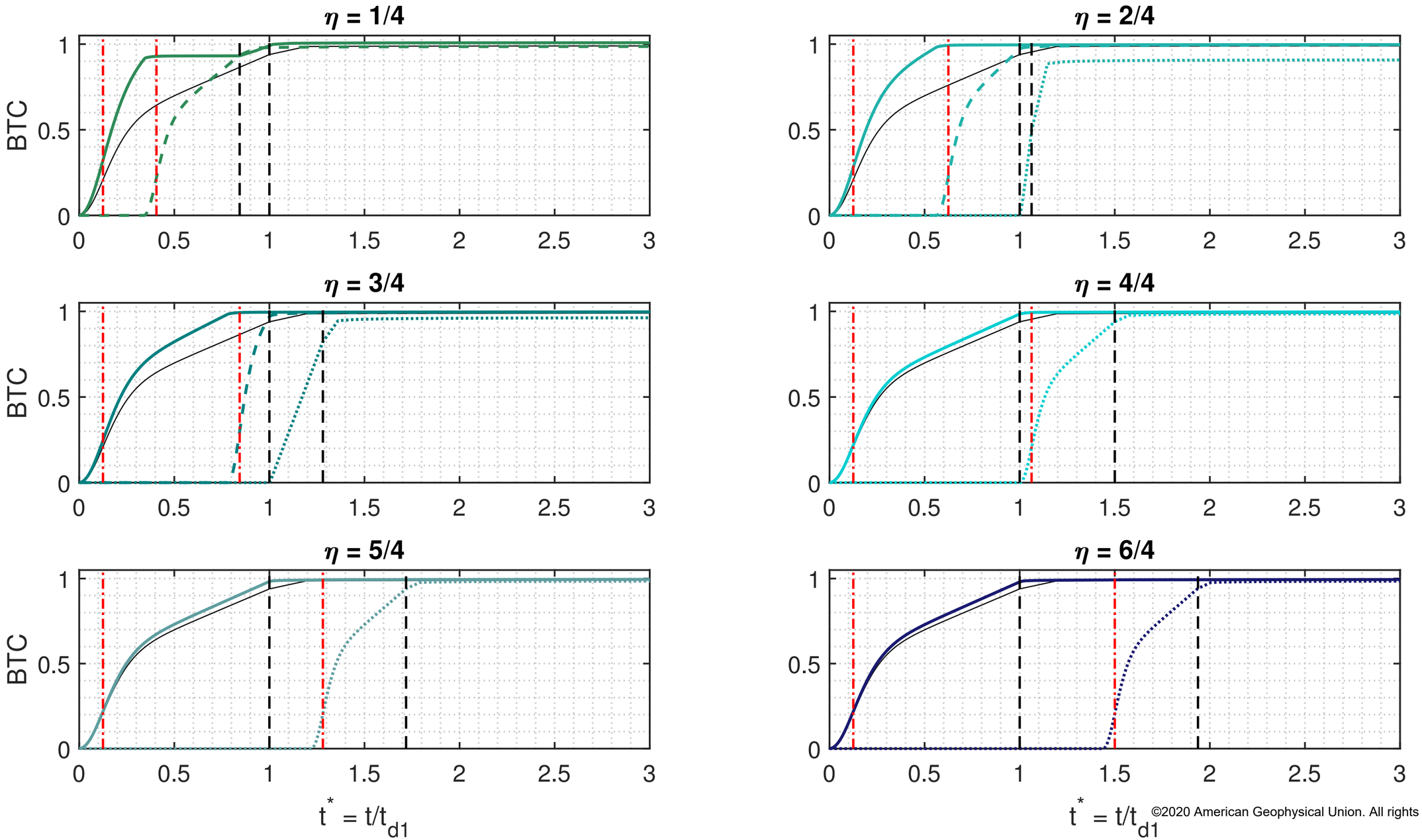

Figure 11.